# 18

# Recognition Imaging Using Atomic Force Microscopy

**Andreas Ebner, Lilia Chtcheglova, Jilin Tang, David Alsteens, Vincent Dupres, Yves F. Dufrêne, and Peter Hinterdorfer**

**Abstract** Recognition imaging using atomic force microscopy (AFM) offers a wealth of new opportunities in biophysical research, such as its ability to localize specific chemical groups and biological receptors on biosurfaces and to measure their molecular-scale interactions. By attaching well-defined chemical groups on tips, it is possible to map chemical properties and interactions on cell surfaces on a scale of a few functional groups. Single-molecule force spectroscopy with tips functionalized with relevant bioligands provides a means of localizing individual receptors and measuring their specific binding forces. Alternatively, recognition sites may also be mapped with unprecedented temporal resolution using dynamic recognition imaging, in which molecular recognition signals are detected during dynamic force microscopy imaging. These AFM modalities, which all have functionalization of the tips with specific molecules in common, provide new avenues for understanding the structure–function of cell surfaces in connection with medical and physiological issues.

## 18.1. Introduction

Molecular recognition involving the specific interaction between receptors and their cognitive ligands plays a pivotal role in life sciences. Signalling cascades, enzymatic activity, genome replication and transcription, cohesion of cellular structures, interaction of antigens and antibodies, and metabolic pathways are just some examples of processes which critically rely on specific recognition. In addition to these specific interactions, nonspecific intermolecular interactions, such as hydrophobic and electrostatic forces, also play essential roles in biological events, such as protein folding and cell adhesion. Force-measuring techniques such as the surface forces apparatus and the optical and magnetic tweezers have been developed to measure these noncovalent intermolecular forces. Although very powerful, these approaches are limited by their poor lateral resolution, meaning that they cannot resolve the spatial distribution of (bio)chemical sites or their interactions. Accordingly, localizing specific chemical

**A. Ebner, L. Chtcheglova, J. Tang, and P. Hinterdorfer** • Institute for Biophysics, Johannes Kepler University of Linz, Altenbergerstr.69, A-4040 Linz, Austria
**D. Alsteens, V. Dupres, and Y. F. Dufrêne** • Unité de chimie des interfaces, Université catholique de Louvain, Croix du Sud 2/18, B-1348 Louvain-la-Neuve, Belgium

P. Hinterdorfer, A. van Oijen (eds.), *Handbook of Single-Molecule Biophysics*,
DOI 10.1007/978-0-387-76497-9_18, 

groups and receptor sites on biological samples and measuring their molecular-scale interactions represents a major challenge in current biophysical research.

In recent years, atomic force microscopy (AFM) has become a powerful tool for probing biosurfaces on the nanoscale [1–5]. Whereas AFM imaging provides three-dimensional views of specimens with (sub)molecular resolution and with minimal sample preparation, AFM force spectroscopy measures the forces within or between single molecules, thereby providing new insights into the molecular basis of crucial biological events such as protein folding and cell adhesion. The AFM works by scanning a sharp tip over the surface of the sample while sensing near-field physical interactions between the tip and the sample. This allows three-dimensional images to be directly generated, even in aqueous solution. The sample is mounted on a piezoelectric scanner that ensures three-dimensional positioning with high accuracy. While the tip (or sample) is being scanned in the ($x$, $y$) directions, the force interacting between tip and specimen is monitored with a sensitivity on the order of piconewtons. This force is measured by the deflection of a soft cantilever that is detected by a laser beam focused on the free end of the cantilever and reflected into a photodiode. AFM cantilevers and tips are typically made of silicon or silicon nitride using microfabrication techniques. The most widely used imaging mode is contact mode, in which sample topography can be measured in two ways. In constant-height mode, the cantilever deflection is recorded while the sample is scanned at constant height. It is often necessary to minimize large deflections to reduce the forces applied to the sample and thus prevent damage. This is achieved in the constant-force mode, in which the sample height is adjusted to keep the deflection of the cantilever constant; thus, the force applied to the tip is maintained at a constant level using a feedback loop. In dynamic or intermittent mode, also known as tapping mode, a tip is oscillated near its resonance frequency and scanned over the surface. The amplitude and phase of the cantilever are monitored and taken as signals for imaging.

In force spectroscopy modalities, such as chemical force microscopy (CFM) and single-molecule force spectroscopy (SMFS), the cantilever deflection is recorded as a function of the vertical displacement of the scanner, that is, as the sample is pushed toward the tip and retracted. This results in a cantilever deflection versus scanner displacement curve, which can be transformed into a force–distance curve by using the appropriate corrections. To gain accurate knowledge about the measured forces, it is important to experimentally determine cantilever spring constants because they may substantially differ from values quoted by the manufacturer [6]. The characteristic adhesion (or unbinding) force between tip and sample observed during retraction may then be used to detect chemical groups (CFM) and receptor sites (SMFS). A few years ago, a novel molecular recognition imaging mode was introduced in which molecular recognition signals were detected during dynamic force microscopy imaging (topography and recognition imaging). This chapter focuses on available molecular recognition AFM modalities, emphasizing methodologies and applications in biophysical research.

## 18.2. Chemical Force Microscopy

Noncovalent interactions, such as hydrophobic and electrostatic interactions, play essential roles in nature because they mediate crucial events such as protein folding and cellular interactions. For the first time, CFM enables researchers to measure these interactions on biosurfaces with nanoscale lateral resolution.

### 18.2.1. Methods

The principle of CFM, which was introduced in 1994, is to use AFM tips with well-defined chemistry for measuring adhesion (or friction) and for imaging surfaces [7,8]. The surface chemistry of commercial tips is poorly controlled and often contaminated with gold and other materials. Therefore, reliable CFM measurements require functionalizing tips with organic monolayers terminated by specific functional groups (e.g., OH or $CH_3$). A common method is based on the formation of self-assembled monolayers (SAMs) of alkanethiols on gold surfaces [9]. This procedure involves coating microfabricated cantilevers with a thin adhesive layer (Cr or Ti) via thermal evaporation, followed by a 15- to 100-nm-thick Au layer. The coated cantilevers are immersed in dilute (0.1–1 mM) ethanol solutions of the selected alkanethiol, followed by a rinse with ethanol, and dried using a gentle nitrogen flow. Although the protocol is fairly simple, it is important to validate the quality of the surface modification, which can be accomplished by treating model supports (glass, mica) in the same way as the tips and by characterizing them by means of surface analysis techniques (e.g., contact-angle measurements or X-ray photoelectron spectroscopy). To minimize surface contamination and alteration it is important to use the functionalized tips immediately after they are prepared.

A CFM experiment typically involves measuring the adhesion strength between chemical groups via force spectroscopy. The cantilever deflection is recorded as a function of the vertical displacement of the piezoelectric scanner, yielding a raw "voltage–displacement" curve that can be converted into a "force–distance" curve. Using the slope of the curves in the region where tip and sample are in contact, one can convert the voltage into a cantilever deflection. The cantilever deflection is then converted into a force $F$ using Hooke's law: $F = -k \times d$, where $k$ is the cantilever spring constant. The curve can be corrected by plotting $F$ as a function of $(z - d)$. The zero separation distance is then determined as the position of the vertical linear parts of the curve in the contact region. The hysteresis or "pull-off" force observed during retraction is used to estimate the adhesion (unbinding) force between tip and sample. Adhesion force maps can be obtained by recording spatially resolved force–distance curves in the $(x, y)$ plane.

Although hydrophobic forces have been known for 70 years and are of prime importance in biology (e.g., in protein folding and aggregation), their detailed mechanisms remain poorly understood. Recently, CFM was shown to be a powerful tool for measuring hydrophobic forces at biological interfaces and for resolving their nanoscale distribution. Figure 18.1 shows the proof of such CFM measurements on model surfaces [10]. SAMs of $CH_3$- and OH-terminated alkanethiols mixed in different proportions were probed using water contact-angle measurements and CFM with hydrophobic, $CH_3$-terminated tips. Consistent with expectations (work of adhesion, Young equation), the contact angle and adhesion force values measured on mixed SAMs increased gradually with the molar fraction of $CH_3$-terminated alkanethiols (Figure 18.1A, B), yielding a linear relationship between the adhesion force and the cosine of the contact angle (Figure 18.1C). This excellent agreement demonstrates that the measured adhesion forces reflect surface hydrophobicity. We point out that, interpretation of the data in terms of interfacial thermodynamics indicated that the measured adhesion forces do not originate from true, direct tip–sample interactions but rather reflect entropy changes associated with the restructuration of water near hydrophobic surfaces. This work is also of practical interest as it shows that CFM can be used for quality control of chemically modified tips, which is not possible when using common analytical techniques. As we discuss later, further interpretation of cellular data requires expressing the measured adhesion

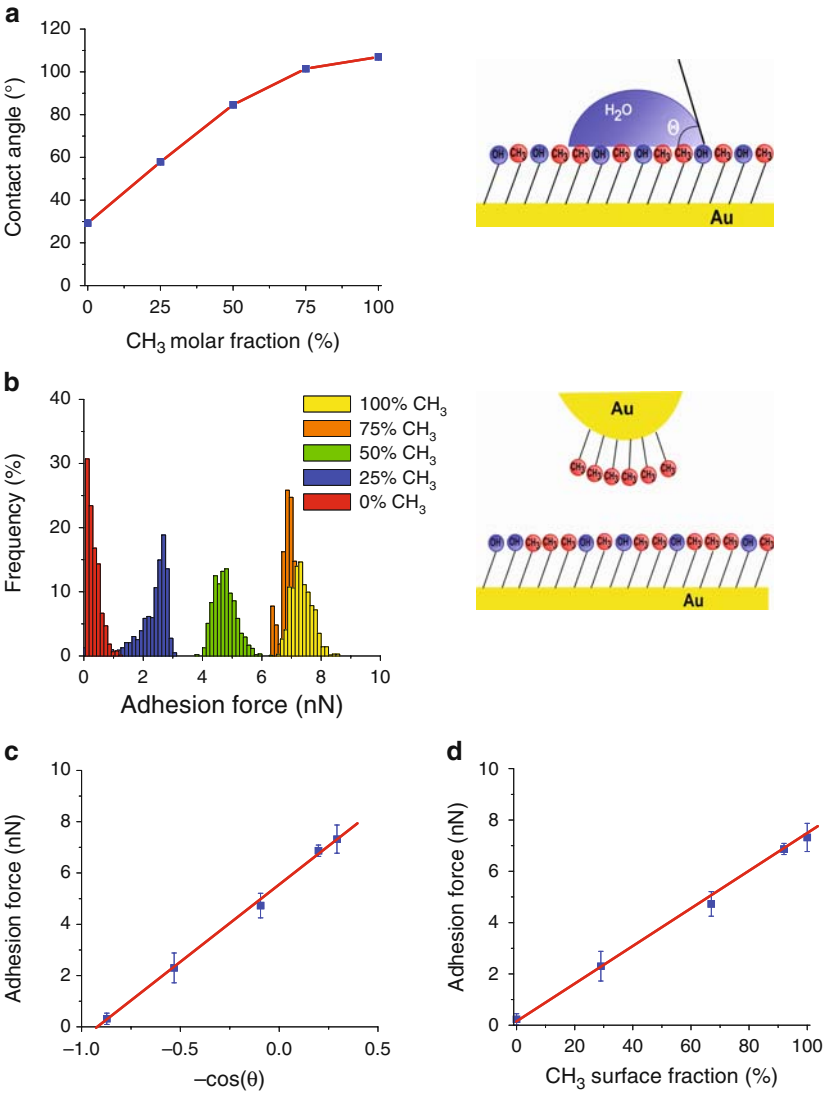


**Figure 18.1.** Measuring hydrophobic forces using chemical force microscopy. **A.** Water contact angle (θ) values measured for self-assembled mixed monolayers of $CH_3$- and OH-terminated alkanethiols as a function of the molar fraction of $CH_3$-terminated alkanethiols. **B.** Histograms of adhesion forces measured on the mixed self-assembled monolayers (SAMs) using hydrophobic $CH_3$ tips. **C.** Variation of adhesion forces as a function of the cosine of the water contact angle. **D.** Adhesion force as a function of the surface fraction of $CH_3$-terminated alkanethiols computed using Cassie's law. (Reprinted with permission from Alsteens et al. [10].)

force as a function of the surface fraction of $CH_3$-terminated alkanethiols, determined using Cassie's law and contact-angle values (Figure 18.1D). CFM with tips bearing charged groups can likewise be used to probe surface charge and electrostatic forces in aqueous solutions [11,12].

### 18.2.2. Chemical Imaging of Live Cells

CFM was recently used in imaging hydrophobic groups on the surface of the human opportunistic pathogen *Aspergillus fumigatus* (Figure 18.2) [9, 13]. Topographic images revealed the presence of regularly arranged rodlets on dormant spores. These structures are composed of hydrophobins, a family of small, moderately hydrophobic proteins that favour spore dispersion by air currents and mediate adherence to host cells. Force curves recorded across these surfaces with a hydrophobic tip showed large adhesion forces of ~3,000 pN magnitude. Comparing the data obtained on reference surfaces (Figure 18.1D) indicated that the conidial surface has a marked hydrophobic character, corresponding to a surface composed of ~10 $CH_3$ and ~15 OH groups, which is fully consistent with the presence of an outermost surface layer of hydrophobins and provides direct indications as to their putative functions as dispersion and adherence structures. In agreement with the uniform surface structure, adhesion maps were rather homogeneous, supporting the notion that the conidial surface is homogeneously hydrophobic.

Dramatic changes of hydrophobic properties can be tracked in real time [14]. A temperature-controlled AFM was used to obtain high-resolution images of the same *A. fumigatus* spore during the course of germination (Figure 18.2). Significant structural alterations were observed, and the rodlet layer changed into a layer of amorphous material, presumably reflecting the underlying polysaccharides. In addition, adhesion maps with hydrophobic tips revealed a dramatic loss of hydrophobicity over time. After 2-hr germination, heterogeneous hydrophobic contrast was observed, reflecting the coexistence of hydrophobic rodlets and hydrophilic polysaccharides. The observed changes are likely to be function related. Whereas the hydrophobic rodlets promote spore dispersion and adhesion to surfaces, the very hydrophilic nature of the germ tube cell wall is likely to favour hyphal growth in aqueous environment.

The impact of drug treatments on the chemical properties of microbes can also be studied using this technique. For instance, the surface of mycobacteria was shown to be uniformly hydrophobic, reflecting the presence of an outermost layer of hydrophobic mycolic acids [10]. This finding is of biomedical relevance because these hydrophobic constituents are thought to represent an important permeation barrier to common antibacterial agents. By contrast, treatment of the cells with drugs targeting specific cell wall constituents lead to a dramatic decrease of cell surface hydrophobicity, attributed to the removal of the mycolic acid layer [15].

In addition to hydrophobicity, surface charge also plays an important role in controlling antigen–antibody, cell adhesion, cell–virus, cell–drug, and cell–ion interactions. This trait can be probed on the nanoscale by using tips functionalized with ionizable carboxyl groups. For the yeast, *Saccharomyces cerevisiae*, force–distance curves were strongly influenced by pH [12]: Whereas no adhesion was measured at neutral/alkaline pH, reflecting the electrostatic repulsion between the negatively charged surfaces, multiple adhesion forces were recorded at low pH values, which are attributed to hydrogen bonding between the protonated tip surface and cell surface macromolecules. These changes were shown to be related to differences in the ionization state of the cell-surface functional groups: The adhesion force versus pH curve was correlated with microelectrophoresis data, with the pH of the largest adhesion force corresponding to the cell isoelectric point.

Hence, CFM is a powerful tool for imaging and quantifying the local hydrophobic and electrostatic properties of cells, thereby complementing the range of methods available for

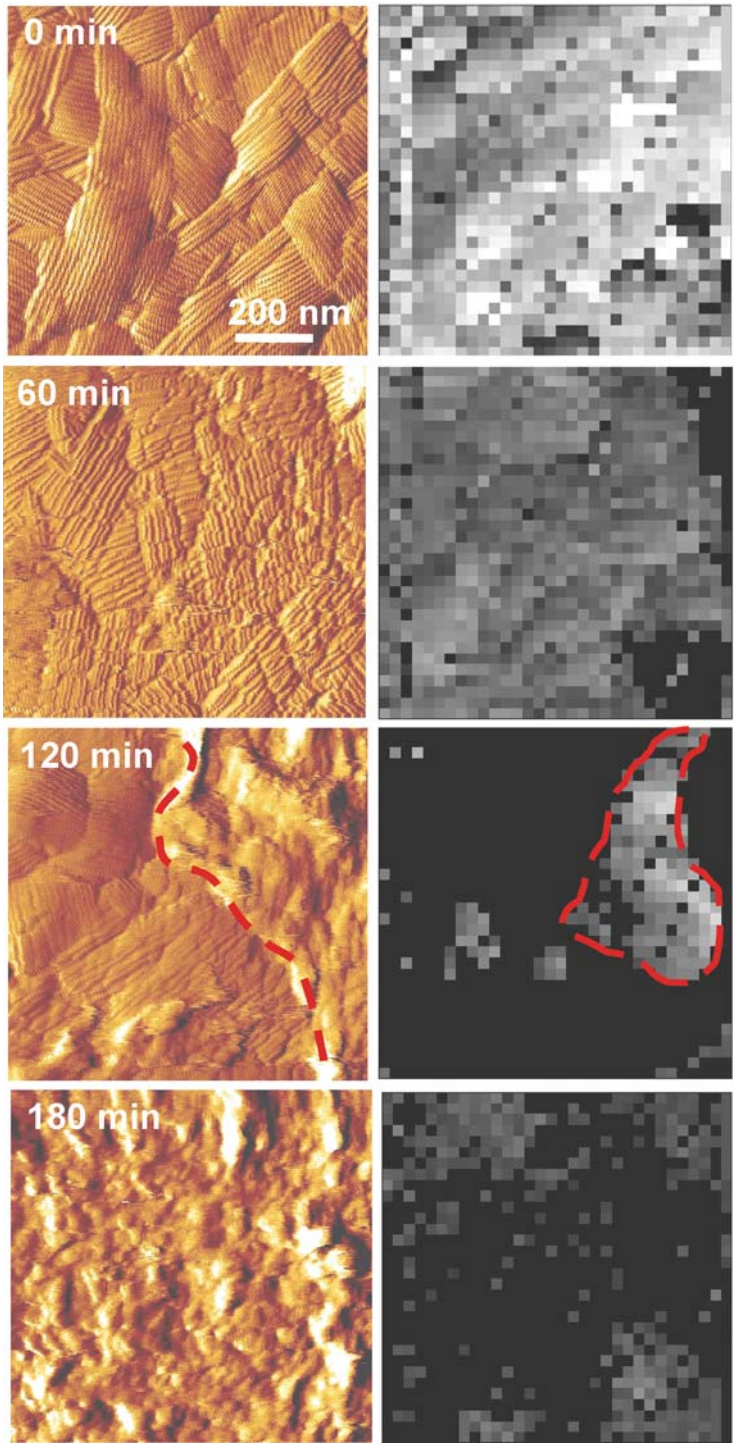


**Figure 18.2.** Chemical force microscopy of single live cells. Series of high-resolution deflection images **(left)** and adhesion force maps **(right)** recorded with a hydrophobic tip on a single *Aspergillus fumigatus* spore during

assessing cell surface properties. A unique feature of CFM is its ability to resolve nanoscale chemical heterogeneities on single live cells.

## 18.3. Recognition Imaging Using Force Spectroscopy

Single-molecule force spectroscopy (SMFS) provides unique possibilities for localizing individual receptors on biosurfaces. In addition, SMFS can measure molecular recognition interactions at the level of single molecules, providing valuable information on molecular dynamics within complexes.

### 18.3.1. Methods

Molecular recognition studies imply functionalizing the tips (and supports) with relevant biomolecules. Several issues should be considered. The forces that immobilize the molecules have to be stronger than the intermolecular force being studied. The attached biomolecules should have enough mobility so that they can freely interact with complementary molecules. The contribution of nonspecific adhesion to the measured forces should be minimized. Attaching biomolecules at a low surface density is recommended to ensure single-molecule detection. Site-directed coupling may be desired to orientate all the interacting molecules in the same way. Immobilization strategies commonly used for making such biological tips are illustrated in Figure 18.3. Using the nonspecific adsorption of biotinylated bovine serum albumin (BBSA), it is possible to measure the interaction between biotin and avidin (or streptavidin) down to the single-molecule level [16,17]. The adsorbed BBSA layer can actually further react with avidin/streptavidin to attach biotinylated molecules [18]. A second approach relies on the strong binding of thiols on gold-coated tips. Whereby proteins, oligonucleotides, and carbohydrates that bear thiol groups can directly be attached on the gold surfaces [19,20], they can also be covalently attached onto SAMs of functionalized alkanethiols on gold by using 1-ethyl-3-(3-dimethylaminopropyl)carbodiimide (EDC) and *N*-hydroxysuccinimide (NHS) [21]. In this context, an interesting approach is to mix long-chain alkanethiols with COOH-terminal functions in a matrix of shorter OH-terminated alkanethiols, which ensures a certain mobility of the attached biomolecules and minimizes nonspecific adsorption [22]. We would like to point out that, it is possible to orientate all biomolecules in the same way by attaching recombinant histidine-tagged proteins onto an AFM tip coated with nitrilotriacetate (NTA)-terminated alkanethiols [23]. This coupling approach offers the advantage of allowing optimal exposure of the C-terminal or N-terminal domains, but it is limited by the rather low binding strength of the NTA–His bond. A third approach is to covalently anchor biomolecules on silicon tips by using various amine-functionalization procedures [24,25]. The amino-terminated surfaces are reacted with a cross-linker that provides the ligands with motional freedom and prevents their denaturation. Cross-linkers typically

**Figure 18.2.** (continued) germination. Within less than 3 hr, the crystalline rodlet layer changed into a layer of amorphous material, presumably reflecting inner-cell-wall polysaccharides. After 2 hr, both rodlet and amorphous regions were found to coexist (separated by dashed line). Consistent with this structural dynamics, substantial reduction of adhesion contrast was noted with time (right images), reflecting a dramatic decrease of hydrophobicity. After 2 hr, heterogeneous contrast was observed in the form of hydrophobic patches (*dashed line*), surrounded by a hydrophilic sea. (Reprinted with permission from Dague et al. [14].)

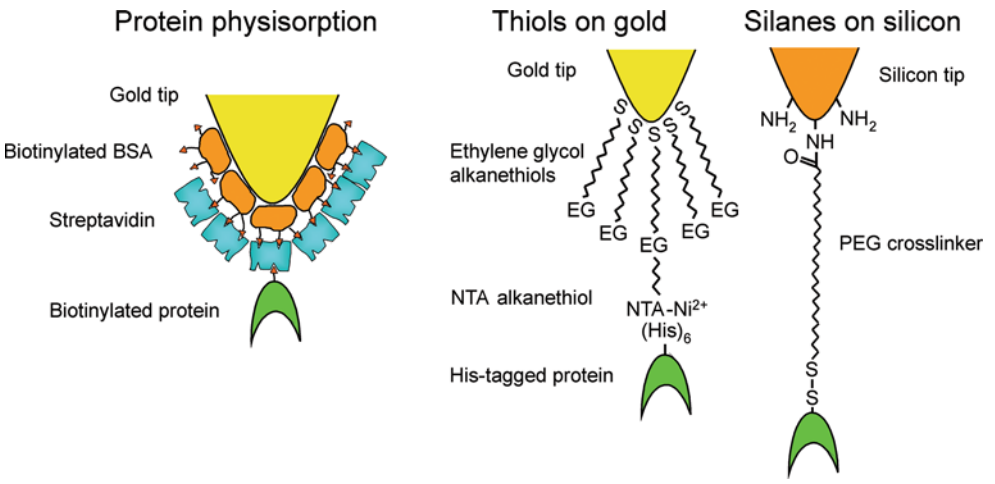


**Figure 18.3.** Strategies commonly used for modifying atomic force microscope tips with biomolecules. **Left to right.** Physisorption of proteins such as biotinylated bovine serum albumin (BSA), chemisorption of alkanethiols on gold, and covalent coupling of silanes on silicon oxide. NTA, nitrilotriacetate; PEG, poly(ethylene glycol). (Adapted with permission from Hinterdorfer and Dufrene [4].)

carry two different functional ends. This can be, for instance, an amine-reactive NHS group on one end for the coupling to tip surfaces and a 2-pyridyldithiopropionyl (PDP) or vinyl sulfone group on the other end, which can be covalently bound to thiol groups contained in ligands.

For cell adhesion studies, animal and microbial cells can be attached onto AFM cantilevers, allowing microscopists to probe various types of cellular interactions. Microbial cells have been immobilized by using glutaraldehyde treatments to create covalent cross-linking between cells and tips [26] or by attaching single cells with a small amount of glue [27]. However, these treatments are likely to affect the structure and properties of the cell surfaces. Alternatively, bacteria can be physically adsorbed onto poly-L-lysine–coated glass beads followed by attachment of the cell-coated beads to a cantilever by using a small amount of epoxy resin [28]. Another elegant approach is to attach individual cells to an AFM cantilever via lectins such as wheat germ agglutinin or concanavalin A, which then allows the measurement of the specific adhesion forces between two adjacent cells [29] or between cells and immobilized ligands [30].

### 18.3.2. Measuring Molecular Recognition Forces

Essentially, molecular recognition using SMFS implies recording force curves between the modified tip and sample, assessing the unbinding force between complementary receptor and ligand molecules from the adhesion "pull-off" force observed upon retraction, and displaying the values either as a histogram or an adhesion map. A typical force curve obtained by using a biotin-modified AFM tip and surface-attached avidin molecules is shown in Figure 18.4A [31]. If the ligand on the tip does not form a specific bond with the receptor on the cell surface, the recognition event is missing and the retrace (Figure 18.4B, blue line) looks like the trace (Figure 18.4B, red line). In addition, the specificity of ligand–receptor binding is usually demonstrated by blocking experiments with free ligands, which are injected into

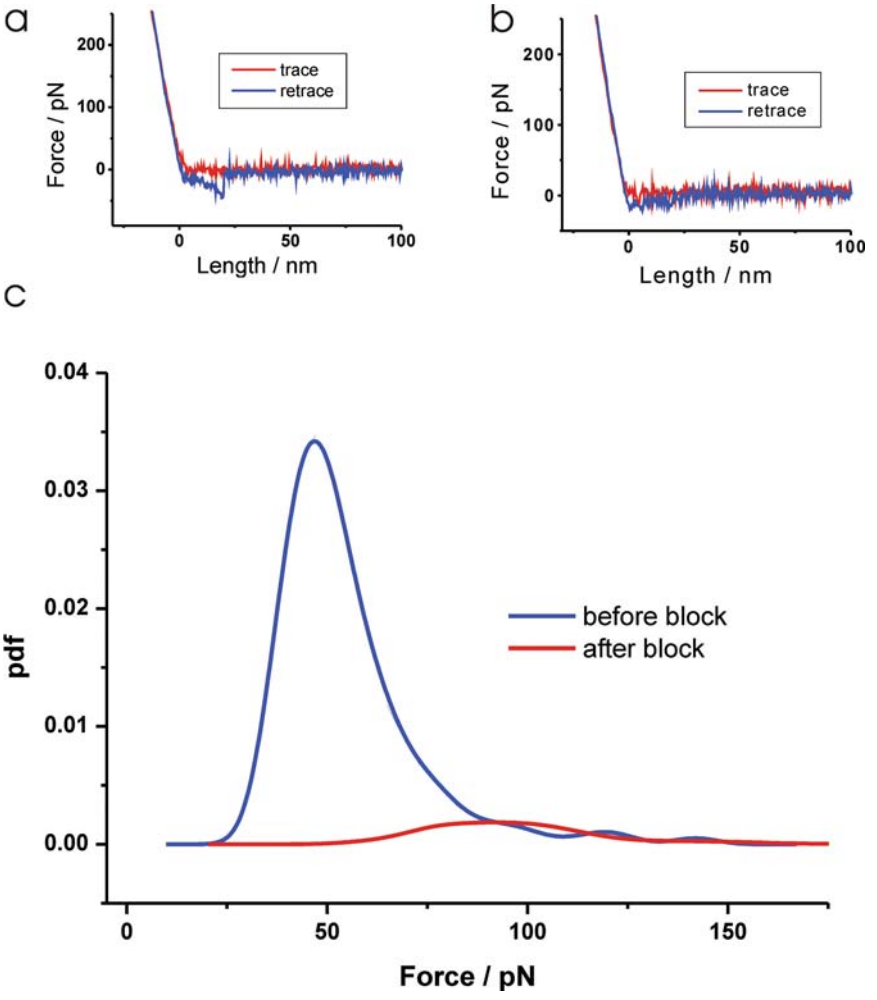


**Figure 18.4.** Typical molecular recognition force spectroscopy data using a biotinylated tip and an avidin-modified surface. **A.** A force–distance circle exhibiting an unbinding event in the retraction period (*blue line*). **B.** This unbinding event disappears when the tip is blocked by adding free streptavidin. **C.** The probability density function (pdf) of the unbinding forces (*blue line*) shows a clear maximum and a high binding probability. In contrast, the streptavidin-blocked tip has a significant lower and broader peak due to the hindered avidin–biotin complex formation. (Adapted from Ebner et al. [31].)

the solution to block the receptor sites on the surface. As a consequence, almost all specific recognition signals completely disappear and only occasional adhesion events are observed.

After acquiring hundreds of force curves, one can construct empirical probability density functions (pdf's) from the detected unbinding forces (Figure 18.4C). The maximum of the distribution reflects the most probable force on which a single ligand–receptor bond dissociates under the force ramp used. An overall binding probability, which is the probability to record an unbinding event, of 19% $\pm$ 6% (Figure 18.4C, blue line) was obtained. Blocking experiments performed by injecting free streptavidin molecules in solution reduced this probability to 2% $\pm$ 1% (Figure 18.4C, red line). No binding was found at all when a bare tip

was used instead of a ligand-coated tip. These results strongly support the specificity of the binding events observed.

Based on such force spectroscopy experiments, a variety of ligand–receptor forces have been measured at the single-molecule level, including those associated with avidin/streptavidin [16,17] antibodies [24,32], DNA [19,33,34], cadherins [35], and bacterial adhesins [23]. Knowledge of these forces contributes to the refinement of our understanding of the molecular basis of molecular recognition events such as those mediating cell adhesion and immunological processes and offers promising prospects in nanobiotechnology for the rapid detection of bioanalytes. Several reports showed that unbinding forces between receptors and ligands depend on the loading rate, that is, the rate at which the force is applied to the bond. We want to point out that, the interaction time may also shift the distribution of adhesion forces towards larger values. For VE-cadherins, this phenomenon was ascribed to the time-dependent association of the protein into complexes with higher-order adhesion strengths [35,36]. For the bacterial adhesin heparin-binding haemagglutinin adhesin (HBHA), the prolonged contact time required to establish strong interaction with heparin was suggested to reflect the time necessary for conformational changes within both molecules to allow an optimal fitting between charged groups [23]. Hence, it is essential in molecular recognition force measurements to vary the loading rate and interaction time to provide reliable data and assess kinetic parameters of the unbinding process.

### 18.3.3. Molecular Recognition Imaging Using SMFS

Molecular recognition imaging using SMFS is comprised of recording arrays of force curves in the $x$, $y$ plane on an area of given size, assessing the unbinding force values for all curves, and displaying them as grey pixels [37]. This method has been applied to different cell types, including red blood cells [38], osteoclasts [39], and endothelial cells [40]. In microbiology, molecular recognition imaging may be used to map adhesion proteins on live bacteria (Figure 18.5) [23]. Bacterial infections are generally initiated by the interaction between adhesins, that is, cell adhesion proteins, on the bacterial pathogen and specific receptors on the host cell surface. A key example is *Mycobacterium tuberculosis*, which adheres to heparan sulphates on epithelial cells via the HBHA. To shed new light on the molecular basis of this interaction, *Mycobacterium bovis* bacillus Calmette-Guérin (BCG) cells expressing HBHA were immobilized on a polycarbonate membrane, an approach that allows live cells to be imaged without using any drying or fixation step (Figure 18.5A). High-resolution images revealed a smooth and homogeneous surface (Figure 18.5B), consistent with earlier scanning electron microscopy observations. Adhesion force histograms (Figure 18.5C) and maps (Figure 18.5D) recorded on cells with a heparin-modified tip revealed adhesion events (bright pixels on the maps) in about half of the locations. The adhesion force magnitude was very close to the value expected for a single HBHA–heparin interaction, supporting the notion that single HBHAs were detected. This was confirmed by showing that a mutant strain lacking HBHA did not bind to the heparin tip. Of interest to, the HBHA distribution was not homogeneous but apparently concentrated into nanodomains, which may promote adhesion to target cells by inducing the recruitment of receptors within membrane rafts. In the future, these molecular recognition studies may help in the development of new drugs capable of blocking bacterial adhesion.

SMFS with antibiotic-modified tips may be used to gain insight into the architecture of bacterial cell walls, as well as into the action mode of antibiotics. In the first such study, AFM tips bearing vancomycin molecules were used to localize single D-Ala-D-Ala–binding

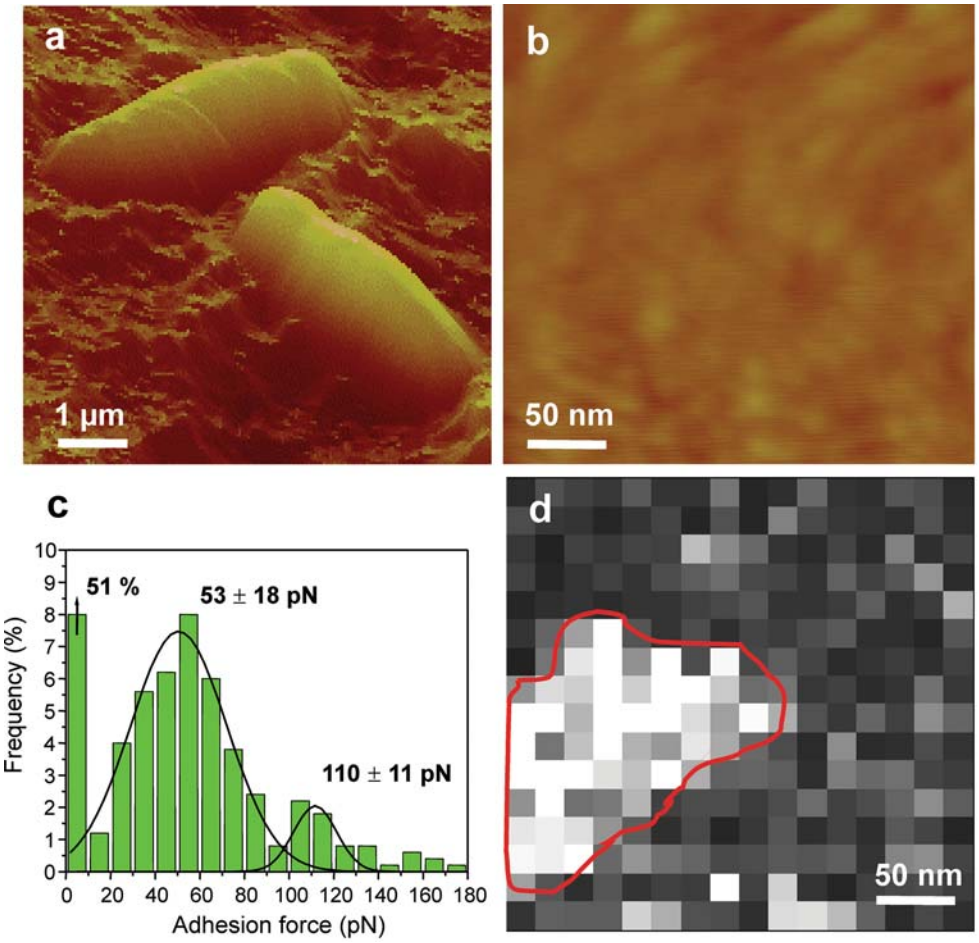


**Figure 18.5.** Imaging single-cell adhesion proteins on live bacteria using spatially resolved single-molecule force spectroscopy. **A.** Topographic image showing two living mycobacteria on a polymer support. **B.** Higher resolution of the cell surface revealing a smooth morphology. **C, D.** Adhesion force histogram and adhesion force map, respectively, recorded on a single cell with a heparin-modified tip. In localized regions, the map reveals adhesion events (clear pixels) due to the presence of adhesion proteins, which seem to be concentrated into nanodomains. (Reprinted with permission from Dupres et al. [23].)

sites up on dividing *Lactococcus lactis* cells [41]. Topographic images of the cells revealed a smooth and elongated cell morphology, as well as a well-defined division septum. Please note, that adhesion force maps recorded with vancomycin-terminated tips demonstrated that the vancomycin-binding sites were essentially located in the septum region, suggesting that newly formed peptidoglycan was inserted in these regions. This was in excellent agreement with fluorescence microscopy images obtained using a fluorescent vancomycin probe.

SMFS also enables researchers to map the distribution of polysaccharides on cell surfaces and to probe their adhesion, elasticity, and conformational properties [42]. For instance, lectin-modified tips were used to pick up and stretch single mannan polysaccharide chains on the two brewing yeast strains, *Saccharomyces carlsbergensis* and *S. cerevisiae* (Figure 18.6) [43]. Polysaccharides were clearly more extended on *S. cerevisiae*, suggesting that not only

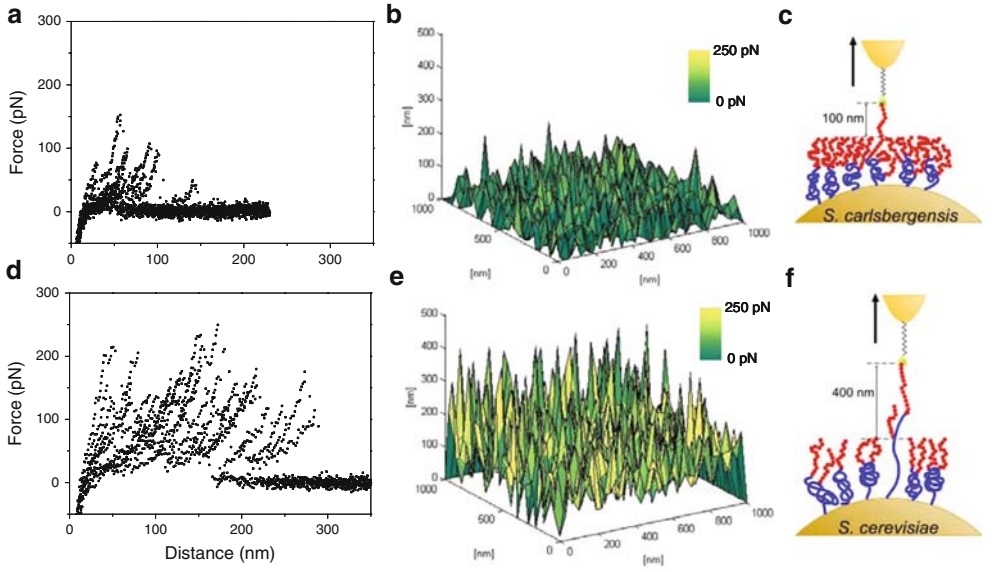


**Figure 18.6.** Localization and conformational analysis of single polysaccharide molecules on yeast using single-molecule force spectroscopy (SMFS). **A, D.** Superimpositions of retraction force curves recorded on *Saccharomyces carlsbergensis* **(A)** and *Saccharomyces cerevisiae* **(D)** yeast cells with an atomic force microscope tip functionalized with the lectin concanavalin A. **B, E**. Three-dimensional maps of polymer properties for *S. carlsbergensis* **(B)** and *S. cerevisiae* **(E)**, showing very different spatial distributions of adhesion forces (false colors; yellow means more adhesive) and of rupture distances (*z* levels). **C, F.** Schematics of the SMFS measurements: Whereas only the mannan oligosaccharides (*red*) are stretched on *S. carlsbergensis*, both the oligosaccharide (*red*) and polypeptide (*blue*) chains of mannoproteins are pulled on *S. cerevisiae*. This may explain why, unlike *S. carlsbergensis* (bottom-fermenting brewing strain), *S. cerevisiae* tends to associate with $CO_2$ bubbles (top-fermenting brewing strain). (Reprinted with permission from Alsteens et al. [43].)

oligosaccharides, but also polypeptide chains of the mannoproteins were stretched. These major differences in polymer properties could explain the very different aggregation properties of the two organisms. In another study, the method was used to reveal the coexistence of polysaccharide chains of different nature on surface of the clinically important probiotic bacterium *Lactobacillus rhamnosus* GG [44]. These SMFS measurements offer exciting prospects for understanding the molecular mechanisms of cell adhesion.

Molecular recognition imaging using SMFS is limited by its poor temporal resolution. The time required to record a molecular recognition image is about a 10 minute segment, depending on the acquisition parameters, which is much greater than the time scale at which dynamic processes usually occur in biology. In the future, progress in developing faster adhesion mapping modes, like the jumping mode [45], will help to circumvent this problem.

## 18.4. Topography and Recognition Imaging

In contrast to common recognition imaging using force spectroscopy, a recently developed imaging technique termed topography and recognition imaging (TREC) [46–52] overcomes some of the limitations regarding lateral resolution and imaging speed by using dynamic force microscopy with a functionalized sensor tip that is oscillated during scanning across the surface.

### 18.4.1. Methods

As a first step, the AFM tips must be upgraded into a molecular sensor by coupling a ligand molecule to the outer end of the scanning tip, preferably through a flexible tether such as poly(ethylene glycol) (PEG) [53]. Because it is an important parameter for adjusting the optimal oscillation amplitude, the length of the PEG tether plays a critical role here. It can range from 8 to 25 ethylene glycol units, corresponding to 3–10 nm of stretched tether length. The immobilization of the sensor molecule via the PEG tether gives the ligand the freedom to adopt the correct orientation so as to facilitate binding to the target molecule on the surface, while the sensor tips scan across the surface. In this approach, the so-called MacMode (Agilent, USA) is used. A magnetically coated cantilever is oscillated through an alternating magnetic field. In contrast to "normal" MacMode imaging, in TREC only the lower part of the oscillation is used to drive the feedback loop for obtaining the topography image. The upper part of the oscillation is used for the generation of the recognition image.

One-dimensional linear scans [52] allow a clear investigation of the nature of the topography and recognition signals. For this purpose, lysozyme molecules were immobilized onto a sample surface at a concentration at which they were singly distributed. The surface was scanned with a bare and with an antilysozyme (HyHel5) functionalized tip, respectively. Figure 18.7A shows the raw signal of a 7-kHz oscillation over a time range of 4 ms. In a presentation of significantly larger time spans of these traces (1 sec, corresponding to one full scan line of 500 nm) the oscillations appeared highly compressed, and only the envelope with the characteristic maxima and minima of each oscillation period remained visible (Figure 18.7B, C). Figure 18.7B shows the result of a scan with a bare tip, that is, a tip containing no antibody. The $z$ positions of the minima varied significantly, and as a result singly distributed bulges with 10–15 nm width and about 1 nm in apparent height appeared along the scan axis. These bulges reflect single lysozyme molecules that resist the further downward movement of the tip towards the mica surface. Their widths and heights are a measure of the apparent molecule size (10–15 nm width, about 1 nm height), and their separation is a measure of the distance between the molecules on the surface (about 35 nm on average). In contrast, the positions of the oscillation maxima remained constant, aside from the minor, randomly occurring variations caused by the thermal noise of the cantilever.

Apparently, the information of the surface topography measured with a bare tip is solely contained in the minima of the cantilever oscillations, and cross-talk between minima and maxima does not exist at the conditions used ($Q$ factor of the cantilever $\sim$1) [54]. Distinct minima were also clearly detected with an AFM tip carrying a specific antibody (Figure 18.7C), indicating that the topography information can also be obtained by using these chemically modified tips. In addition, however, the maxima were also significantly affected (Figure 18.7C). The antibody of the AFM tip binds to the specific antigenic sites on lysozyme during scanning, and the physical connection temporarily established between tip and substrate thereby reduces the upstroke of the cantilever oscillation. As a further consequence, recognition of lysozyme by the tip-conjugated antibody results in reduction of the oscillation maxima, which allows for detection of the lateral position of specific binding sites.

Topography and recognition images can be simultaneously obtained using a specially designed electronic circuit (PicoTREC, Agilent, Chandler, Arizona). The principle of TREC (Figure 18.8A) is hereafter explained. The time-resolved deflection signal of the oscillating cantilever is low-pass filtered to remove the thermal noise, DC-offset levelled, and amplified before it is split into the lower ($U_{\text{down}}$) and ($U_{\text{up}}$) upper parts of the oscillations. The signal passes a trigger threshold on each path, and the lower and upper peak of each oscillation

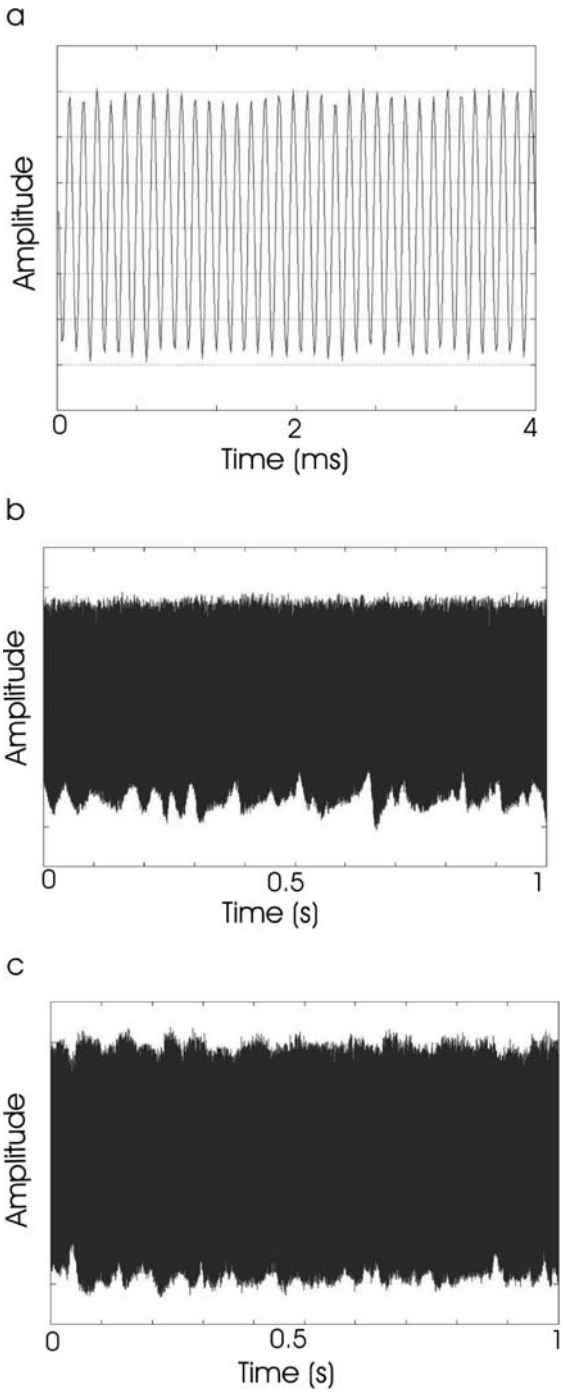


**Figure 18.7.** Deflection signals of magnetically oscillated cantilevers using disabled feedback. **A.** Oscillations signals over a time range of 4 sec with a peak-to-peak amplitude of ~5 nm. **B, C.** Full line traces over 500 nm (in 1 sec) with a bare tip and using a ligand-tethered tip, respectively. (Reprinted with permission from Stroh et al. [52].)

period is determined by means of sample and hold analysis. Succeeding peaks result in a staircase function, which is subsequently filtered and fed into the controller of the microscope, with $U_{down}$ driving the feedback loop to record the height (i.e., topography) image and $U_{up}$ providing the data for constructing the recognition image. If cantilevers with low $Q$ factor ($\sim$1 in liquid) driven at frequencies below resonance are used, both types of information are independent. In this way, topography and recognition images can be recorded simultaneously and independently.

TREC imaging was applied to singly distributed avidin molecules by using a biotinylated tip (Figure 18.8B, C). The tip oscillation amplitude (8 nm) was chosen to be slightly

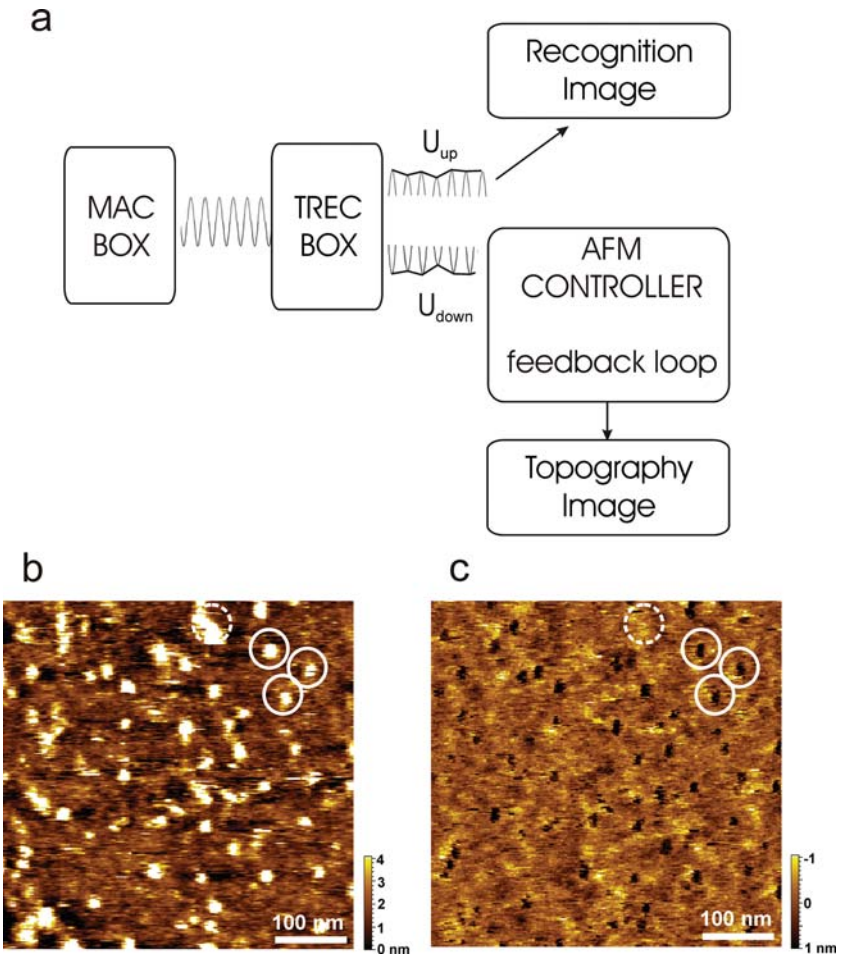


**Figure 18.8.** Topography and recognition imaging (TREC) signal processing. **A.** The raw cantilever deflection signal is fed into the TREC box, where the maxima ($U_{up}$) and the minima ($U_{down}$) of each oscillation period are depicted and used for the recognition and the topography image, respectively. AFM, atomic force microscope; MAC, magnetic alternating current mode. (Reprinted with permission from Stroh et al. [52].) **B, C.** Topographic and recognition images, respectively, using a biotin-functionalized tip. In the topographic image, single avidin molecules electrostatically adsorbed to mica are observable. In the simultaneously acquired recognition image, recognition events appear as black spots, showing a good correlation to the corresponding topography. (Reprinted with permission from Ebner et al. [66].)

smaller than the extended PEG cross-linker length (10 nm) through which the biotin was coupled to the AFM tip. Thus, both the biotin remained bound while passing a binding site and the reduction of the upwards deflection was of sufficient significance compared to the thermal noise. Because the spring constant of the polymeric cross-linker increases nonlinearly with the tip–surface distance, the binding force is only sensed close to full extension of the cross-linker (given at the maxima of the oscillation period). Therefore, the recognition signals are well separated from the topographic signals arising from the surface both in space ($\Delta z \sim$ 5 nm) and time (half-oscillation period $\sim$0.1 ms).

The visible bright dots with 2–3 nm in height and 15–20 nm in diameter in the topography image (Figure 18.8B) represent single avidin molecules stably adsorbed onto the flat mica surface. The recognition image shows black dots at positions of avidin molecules (Figure 18.8C) because the oscillation maxima are lowered due to the physical avidin–biotin connection established during recognition. The lateral positions of the avidin molecules obtained in the topography image are spatially correlated with the recognition signals of the recognition image. (circles in the images (Figure 18.8B, C)). Recognition between the biotin on the tip and the avidin on the surface took place for almost all avidin molecules (for exception, see dotted circle in Figure 18.8C). Thus, one would assume to have almost all binding epitopes oriented away from the mica surface and accessible to the biotin on the tip, resulting in a high binding efficiency.

In addition, the tether length (10 nm) via which the biotin was bound to the AFM tip was greater than the oscillation amplitude (8 nm) so that the biotin on the tip always had a chance to bind to the avidin when passing a binding site during lateral scans. Biotin–avidin recognition resulted in a reduction of the oscillation amplitude, and, indeed, due to the close proximity of the tip to the surface, the binding efficiency was high. It is important to note that topography and recognition images can be recorded at speeds typical for standard AFM imaging and are therefore considerably faster than conventional force mapping.

### 18.4.2. Applications of TREC Imaging

#### Chromatin

The fundamental particle of the chromatin structure—the nucleosome—is a self-assembled complex of basic histone proteins wrapped by approximately two turns of DNA. Using conventional AFM, it is challenging to identify and distinguish the single components because this technique only yields the shape and volume of the structures, which does not heavily depend on the molecular weight. In contrast, TREC allows recognition of a specific type of molecule in a complex structure while simultaneously yielding high-resolution topographic images. This strategy recently localized, histones H3 in remodelled chromatin structures [48]. For this procedure, nucleosomal arrays containing the mouse mammary tumor virus (MMTV) promoter region were salt-reconstituted and subsequently deposited on glutaraldehyde aminopropyltriethoxysilane (GD-APTES)–treated mica. Polyclonal anti–histone H3 antibodies were thiolated and attached to a PEG tether on the end of an AFM tip. Topographic and recognition images of nucleosomal arrays were simultaneously recorded using this tip. The dark recognition patches and the pattern in which they occur clearly coincided with the positions of the nucleosomes in the topographic image because histone H3 is one of the proteins that constitute the core of each nucleosome.

The specificity of the recognition process was tested by injecting exogenous proteins into the liquid cell in which the sample was imaged. When a BSA solution was added, the

recognition image remained unaffected. However, if a similar concentration of a peptide corresponding to amino acids 1–20 of the N-terminal tail of histone H3 was injected into this sample, the recognition signal was completely abolished. Thus, the ability of the tip-tethered antibody to produce a recognition signal was blocked by an excess of its specific antigen in solution, demonstrating that the recognition signals came from specific interactions between the antibody on the tip and its antigen on the surface. The major impact of TREC comes from its ability to monitor specific components in heterogeneous samples while they undergo biological processes. In such experiments, hSwi-Snf and chromatin were incubated together and then deposited onto mica. *In situ* images of the same nucleosomal arrays were taken before ATP was added (hSwi-Snf is inactive) and after ATP addition (hSwi-Snf is activated). The progress of remodelling was therefore tracked on individual molecules. Comparison of recognition images before and after ATP addition showed a variety of remodelling and compositional changes.

TREC on chromatin was also explored using another kind of recognition molecule, the DNA aptamer [55]. These are small, stem-loop, single-stranded DNA molecules generated via systematic evolution of ligands by exponential enrichment. Aptamers consist of a single strand of DNA and are therefore easy to synthesize and store. They are easily folded by thermal annealing in an appropriate buffer and can also be easily attached to an AFM tip by using commercially available DNA that is chemically modified at one end. Aptamers may be as specific as antibodies and have a high affinity for some small molecules. A proof-of-principle TREC study using aptamers as ligands with immunoglobulin E as receptor was performed [55] before histone H4 aptamers were investigated to elucidate their specificity to different histone classes [56].

Using an *in vitro* selected aptamer for histone H4, a series of recognition imaging experiments against recombinant histone H3, H2A, and H2B were performed. It was shown that the H4 aptamer recognized the H4, H3, H2A, and H2B proteins with recognition efficiencies of 80%, 29%, 3%, and 5%, respectively. The low level of recognition to the H2A and H2B proteins correlated with previous affinity measurements performed on the histone tail sequences. Comparison of different tail sequences revealed a GGX motif that was present, twice in H4 tails and once in H3 tails, but was absent from the H2A and H2B tail sequences. It thus appeared likely that this motif is important in aptamer binding. Because it was found that DNA aptamers represent a viable alternative to traditional antibodies in recognition imaging microscopy, it was suggested that this approach could be used to study key epigenetic modifications involved in chromatin remodelling [56].

## Bacterial Surface Layers

Crystalline bacterial surface layers (S-layers) represent a unique self-assembly system optimized during billions of years of biological evolution [57–60]. The intrinsic ability of S-layers to self-assemble allows for *in vitro* formation of isoporous two-dimensional (2D) protein lattices in suspension, on lipid films, on liposomes, and on solid supports [57,61]. Strep-tagII, an eight–amino acid peptide and artificial ligand for Strep-Tactin (a genetically engineered streptavidin variant with higher affinity towards Strep-tagII than streptavidin [62]), was fused to a C-terminally truncated form of the S-layer protein SbpA of *Lysinibacillus sphaericus* CCM 2177. SbpA is one of the most extensively studied S-layer proteins, with the ability to self-assemble into a square (p4) lattice [57,61,63,64]. In previous studies, it was found that the fused Strep-tagII did not interfere with the self-assembly properties of S-layer

fusion protein SbpA–Strep-tagII and that the Strep-tagII was located on the exposed surface of the S-layer lattice [65].

We applied TREC for lateral imaging of the recognition sites on the nanoarray, to identify the location of Strep-tagII in the square S-layer lattice with nanoscale resolution. The AFM tip was covalently functionalized with Strep-Tactin via a short, elastic linker. The topography images of the nanoarrays with mixed S-layer proteins rSbpA–Strep-tagII and SbpA were acquired with MAC mode AFM. The 2D nanoarrays of mixed S-layer proteins with square lattice and with a center-to-center spacing of ∼14 nm, typical for the S-layer protein SbpA [60,65], could be observed in the topography images (Figure 18.9A). Figure 18.9B shows the simultaneously acquired recognition image generated by scanning with a Strep-Tactin–coupled AFM tip over the surface of mixed rSbpA–Strep-tagII/wild-type SbpA (1/7) lattice. When Strep-Tactin on the tip recognized Strep-tagII, the oscillating tip response was altered, and this change was converted into a recognition signal [48,66] that displayed the location of Strep-tagII in the S-layer nanoarrays. The dark spots in the recognition image (Figure 18.9B) indicate where recognition events between Strep-Tactin and Strep-tagII occurred and reflect the distribution of the fusion protein rSbpA–Strep-tagII in the cocrystallized S-layer lattice consisting of rSbpA–Strep-tagII/wild-type SbpA. Although the dark

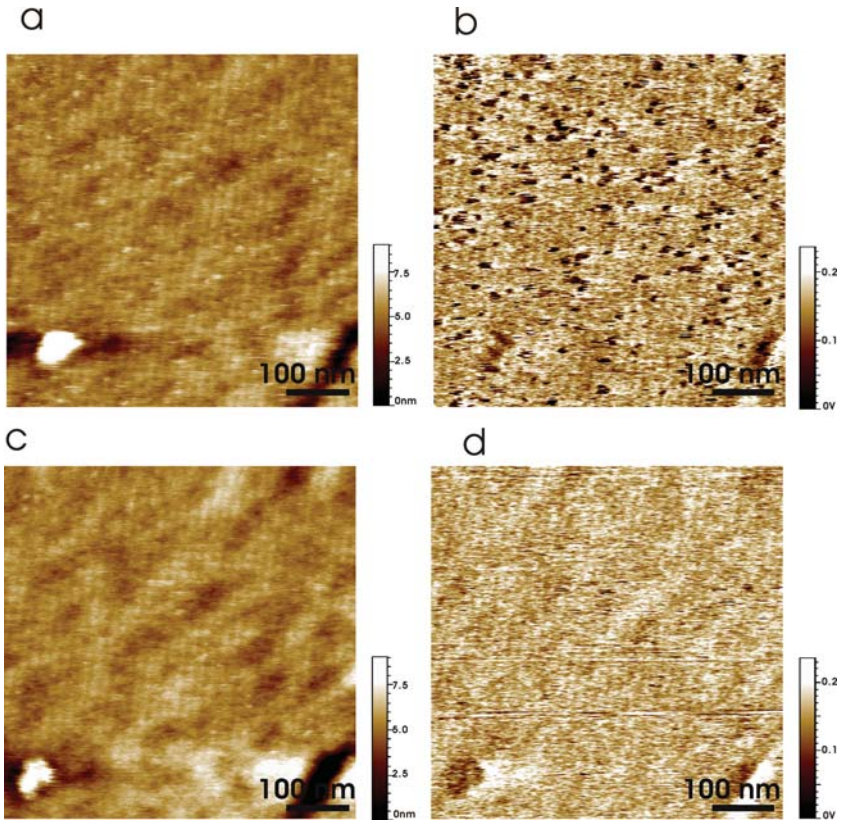


**Figure 18.9.** Topography and recognition images of surface-layer in the absence and presence of blocking agents. **A, B.** Topographic and recognition images, respectively, of the surface-layer proteins rSbpA–Strep-tagII and wild-type SbpA cocrystallized (in a molar ratio of 1:7) on a silicon chip. **C, D.** Topographic and recognition images acquired after Strep-Tactin on the atomic force microscope tip was blocked by adding free Strep-tagII.

spots were located all scattered over the nanoarray surface of the cocrystallized S-layer proteins, they were randomly located. The specificity of the recognition signals was proven by acquiring topography and recognition images at the same place after blocking Strep-Tactin on the tip (Figure 18.9C, D). The dark spots in the recognition image were completely abolished after injection of free Strep-tagII into the AFM fluid cell during imaging (Figure 18.9D). In this case, the ability of the tip-tethered Strep-Tactin to acquire a recognition signal was blocked by the excess of Strep-tagII in solution. This proved that the recognition signals shown in Figure 18.9B arose from specific interaction between Strep-Tactin coupled to the AFM tip and Strep-tagII on the surface of the cocrystallized S-layer lattice.

Subsequently, a smaller scan area on the surface of the cocrystallization of rSbpA–Strep-tagII and SbpA was imaged to increase the lateral resolution. Figure 18.10A, B show the simultaneously acquired topography and recognition images, with a scan size of 216 nm. To precisely localize the position of Stre*p*-tagII, a "center-of-mass" approach was used. In this case, the center-of-mass approach determined the position of the symmetry point, which was identified as the recognition site. Even though the diameter of the recognition spot was on the order of two times the length of PEG and protein (∼7 nm), the position of the recognition spots was determined with accuracy of less than 1 nm. By overlaying the position of Strep-tagII in recognition spots and the topography image (Figure 18.10C), 88% of the position of Strep-tagII in recognition spots were found on the corner of the square lattice, which indicated the location of Strep-tagII in the lattice of S-layer. Figure 18.10D shows a schematic drawing of the cocrystallization of rSbpA–Strep-tagII and wild-type SbpA and

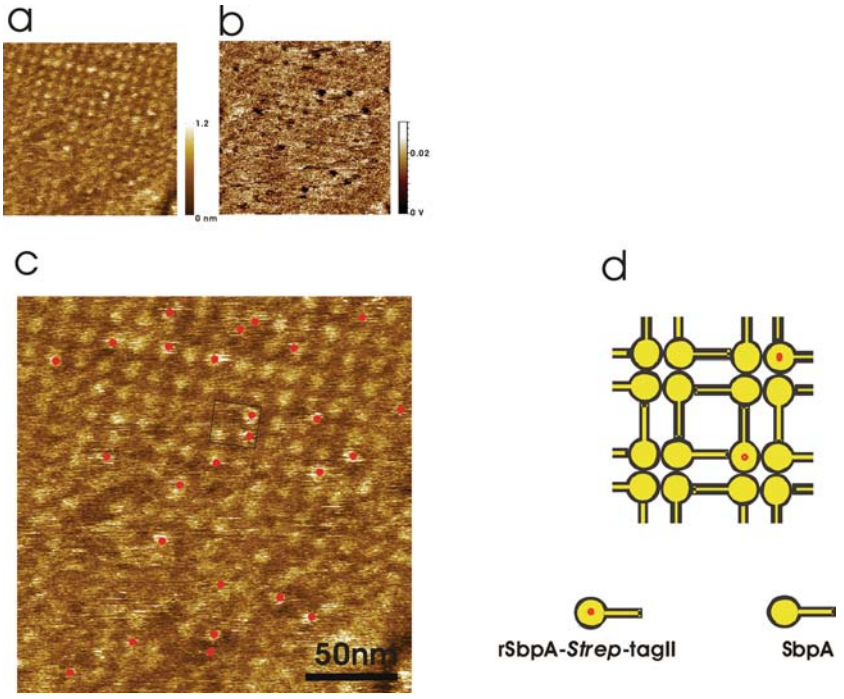


**Figure 18.10. A, B.** Topographic and recognition images, of the surface-layer proteins rSbpA–Strep-tagII and SbpA (in a molar ratio of 1:7) cocrystallized on a silicon chip. **C.** Superimposition of a recognition map of Strep-tagII onto the corresponding topographic image. **D.** Schematic drawing of cocrystallized rSbpA–Strep-tagII and wild-type SbpA.

represents the square area in Figure 18.10C. The red spot indicates where the Strep-tagII was located in correspondence to the dark spots in the recognition image. These results demonstrate that Strep-tagII was exposed on the surface of the S-layer lattice and located in the corner of the square S-layer lattice.

## Membranes

In a recent study, the distribution of cystic fibrosis transmembrane regulator (CFTR) molecules in red blood cell membranes was investigated. CFTR is a chloride channel and a regulator protein for several membrane conductases [67]. It maintains the salt and water balance on the epithelium and regulates processes such as cell volume regulation [68]. CFTR dysfunction results in a severe disease, namely cystic fibrosis (CF). It is the most common genetic disease in people and is characterized by impaired epithelial transport mainly in the respiratory system, pancreas, and liver. The most typical mutation is the deletion of the amino acid phenylalanine at position 508, resulting in the misfolded protein (F508del CFTR). This leads to impaired trafficking to the plasma membrane. As a result, the number of CFTR molecules in the plasma membrane is strongly reduced [69,70]. There is strong evidence that CFTR is not only expressed in epithelia but also in human erythrocytes [71–76]. In this context, TREC imaging was used to accurately map CFTR sites directly on erythrocyte membranes.

Before starting with the TREC experiments the erythrocyte membrane preparation was investigated by dynamic force mode imaging by using a bare cantilever. The membranes appear as round, flat structures with a diameter of $\sim$10 $\mu$m and up to 25 nm in height. For TREC imaging, an anti-CFTR antibody was covalently coupled to an AFM tip via a lysine residue. The TREC measurements were performed on erythrocyte membranes of healthy (non-CF) and CF-positive patients, respectively. Topographic images of both non-CF (Figure 18.11A) and CF (Figure 18.11D) erythrocyte membranes revealed similar structures protruding out of the membranes with 10–12 nm in height, representing membrane proteins. These structures were comparable to the topographic measurements using an unmodified AFM tip with similar specifications. Visualization at single-molecule level was achieved without compromising its topographic imaging performance, despite the fact that the tip was carrying a tethered antibody. The simultaneously acquired recognition images (Figure 18.11E) showed dark spots, corresponding to interactions between the specific anti-CFTR antibody on the tip and the CFTR membrane proteins. These binding sites can be assigned to particular topographic structures, allowing the identification of CFTR among the abundance of different proteins present in the membrane.

The size of recognition spots for CF and non-CF membranes was 32 $\pm$ 5 and 33.5 $\pm$ 8 nm, respectively. The lateral resolution of TREC is limited by PEG-antibody-ligand system, which causes a lateral mobility of the antibody restricted by the linker length. The configuration used allows an antigen–antibody binding in a distance of up to $\sim$12 nm (linker length plus antibody) to the tip apex. Because the recognition signals were recorded relative to the tip position, a single antigen could generate a recognition spot with a diameter of up to 24 nm. The tip radius also contributes to the signal broadening, so that the overall diameter of a recognition spot could be up to 30–35 nm. Taking this into account, we see that the observed recognition spots with diameters of about 33 nm revealed the presence of at least one CFTR molecule. Although the cluster formation plays an important role, the exact number of CFTR molecules in one recognition spot cannot be given. Nevertheless, it could clearly be shown

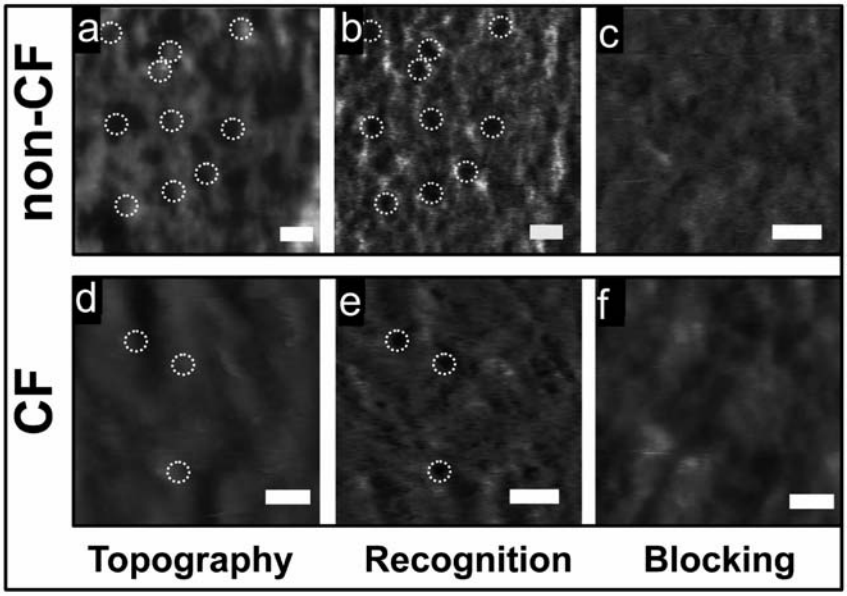


**Figure 18.11.** Topographic and recognition images of isolated erythrocyte membranes. Non–cystic fibrosis (CF) **(A)** and CF-positive **(D)** erythrocyte membranes show molecular recognition events **(B, E)** when scanned with an anti–cystic fibrosis transmembrane regulator (CFTR)–functionalized sensor tip. Specificity proof experiments using free anti-CFTR antibodies in solution show no recognition events **(C, F)**. Scale bar × nm.

that CF samples (Figure 18.11E) clearly revealed fewer recognition spots compared to non-CF ones (Figure 18.11B). Quantification of the recognition events revealed values of 6.2 ± 1.29 ($n = 4$) and 1.9 ± 0.90 ($n = 12$) CFTR molecules per $\mu m^2$ for non-CF and CF erythrocytes, respectively (mean ± SD). By extrapolation to the total erythrocyte surface area of 130 $\mu m^2$, one can estimate ~800 CFTR molecules/erythrocyte for non-CF samples and about 250 CFTR molecules/erythrocyte for CF samples (if multimeric clustering in one recognition spot is neglected).

To test the specificity of recognition, an excess of free anti-CFTR antibodies was injected into the measurement fluid chamber. This resulted in a hindering of tip–antibody surface–antigen complex by forming a CFTR–anti-CFTR antibody complex. Thus the free CFTR antibodies were bound to the membrane-embedded CFTRs, which hindered tip–antibody surface–antigen complex formation. As a result, in the TREC measurements, the recognition spots disappeared in the recognition image with an efficiency of more than 90% due to abolishment of the reduction of the upper oscillation amplitude (Figures 18.11C, F), whereas the sample topography was unaffected.

TREC recognition imaging allowed an accurate identification of CFTR within the plasma membrane at the single-molecule level. This provides considerable advantages because it removes the data-averaging drawback inherent in the conventional techniques that record measurements over large ensembles of molecules. With further advances in the TREC technique (increasing spatial resolution, improving sample preparation) this method provides more detailed information on protein clustering in native membranes. Moreover, elucidating the distribution of single proteins and their organization within the plasma membrane becomes feasible.

## Cells

Real-time visualization and quantification of receptor-binding sites on cell surfaces is a fundamentally challenging task in molecular cell biology. The first TREC studies on cells were performed on microvascular endothelial cells of mouse myocardium (MyEnd) to locally identify vascular endothelial (VE)-cadherin binding sites and colocalize the receptor position with membrane topographic features [50] (Figure 18.12A). White VE-cadherin belongs to the widespread family of cadherins, transmembrane glycoproteins are known to play an important role in calcium-dependent homophilic cell-to-cell adhesion. VE-cadherin is located at intercellular junctions of essentially all types of endothelium, where VE-cadherin molecules are clustered and linked through their cytoplasmic domain to the actin cytoskeleton. The cadherin *cis*-dimer, which is formed by the association of two extracellular domains in physiological $Ca^{2+}$ concentration (1.8 mM), represents a basic structural functional unit to promote a homophilic bond between cells [77].

To avoid lateral diffusion of VE-cadherin and increase the stability of the cell membrane, cells were gently fixed with glutaraldehyde, which is not only suitable for preventing the lateral mobility of receptors on the cell surface, but also maintains cell volume and generally preserves the filamentous structure on the cell cortex. TREC measurements were conducted with magnetically coated AFM tips (MAC tips), which were functionalized with a recombinant VE-cadherin–Fc *cis*-dimer via a soft and long (∼8 nm) PEG linker. Recognition signals correspond to the amplitude reduction due to a binding between VE-cadherin molecules on the AFM tip and the cell surface when specific *trans*-interaction occurs (seen as dark spots in recognition image). These dark spots are distributed nonuniformly and represent microdomains with dimensions from ∼10 to ∼100 nm (Figure 18.12B). Figure 18.12B illustrates high recognition efficiency, which remains practically unalterable on subsequent rescans. The addition of 5 mM ethylenediaminetetraacetic acid ($Ca^{2+}$-free conditions) leads to the disappearance of almost all binding events in the recognition image, whereas no change in the topography image is observed. A closer look at some recognition spots reveals that they consist of one to two large domains (50–80 nm) surrounded by smaller domains (10–20 nm) or even single-molecule spots (typically 1–4 pixels long; 1 pixel ∼4 nm) (Figure 18.12B). Given the size of the VE-cadherin *cis*-dimer (diameter 3 nm) and the free orientation of PEG linkers leading to specific binding even before/after (8 nm) the binding-site position, the dimensions of the single sites reflect the expectation. More than 600 single events were recognized and ∼6,000 active *cis*-dimers were estimated over the scanned area (4 $\mu m^2$). The shapes and the positions of VE-cadherin domains were correlated with topographic features of MyEnd cell surfaces. The topography of a scanned MyEnd cell surface area represents a complex picture of linear and branched filamentous structures, likely representing filaments of the peripheral actin belt and some globular features as well. We point out that, a few VE-cadherin domains were found directly on top of filaments. Nevertheless, most domains were located near and between filaments, indicating that at this stage of cell maturation (day 1 or 2 after seeding), clustering of VE-cadherin was incomplete.

In another study, TREC was used to visualize vascular endothelial growth factor receptors (VEGFRs) [78] on vascular endothelial cells. VEGFR is a transmembrane receptor tyrosine kinase, which is primarily expressed in vascular endothelial cells and plays an important role in mechanosensory functions such as focal adhesion turnover, actin cytoskeletal remodelling, and angiogenesis. Intermittent blocking of VEGFR2 in vascular endothelial cells promotes rapid blood vessel regression in animal models, but new strategies to inhibit/promote this signalling require enhanced understanding of VEGFR2 distribution and binding kinet-

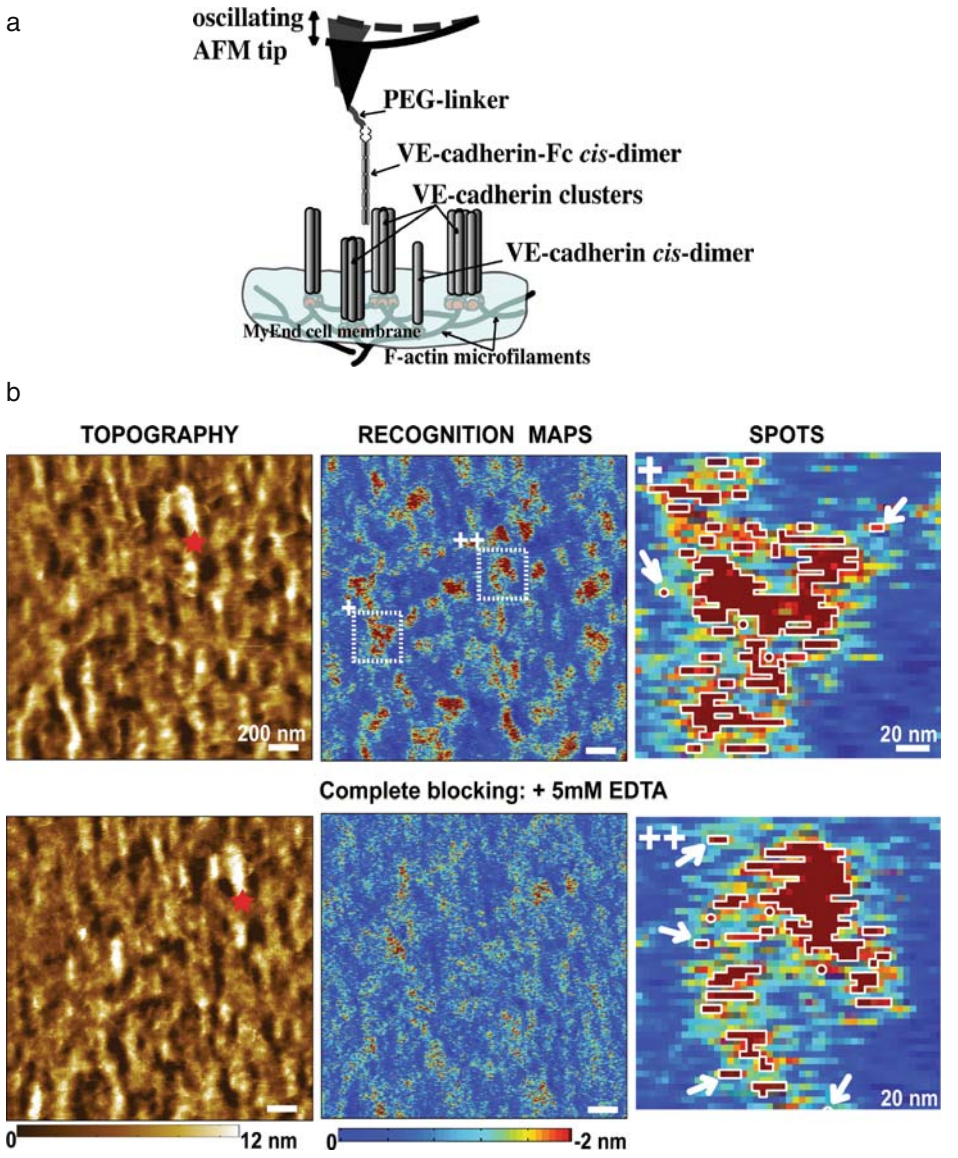


**Figure 18.12. A.** Scheme of dynamic recognition imaging for visualizing VE-cadherin–binding sites (here single *cis*-dimers and/or clusters) on a gently fixed MyEnd cell surface. **B.** Simultaneously recorded topography and recognition (TREC) images of a MyEnd cell surface obtained with VE-cadherin-Fc–functionalized tip. The addition of 5 mM ethylenediaminetetraacetic acid led to the disappearance of recognition clusters as the active VE-cadherin-Fc *cis*-dimers on the atomic force microscope (AFM) tip dissociated into inactive monomers, thereby abolishing specific VE-cadherin *trans*-interaction. After blocking experiments, topography remains unchanged, indicating that blocking does not affect membrane topography. Red stars in the topographic images show the AFM scanner lateral drift of ~5 nm/min. +, ++, Examples of recognition spots magnified from recognition image. Recognition areas are depicted by threshold analysis (threshold = – 1.7 nm) and bordered by white lines. Single VE-cadherin *cis*-dimers can be clearly detected (*arrows*). PEG, poly(ethylene glycol).

ics with biological or synthetic molecules. To identify VEGFR2 receptors, TREC imaging was performed on chemically fixed human umbilical vein endothelial cells (HUVEC) that endogenously express VEGFR2. By scanning the cell surface with a MAC tip tethered with monoclonal anti-VEGFR2 antibodies, dark regions with a diameter of $45.9 \pm 8.9$ nm were observed. These domains were assumed to be putative receptor locations that were consequently confirmed through the demonstration of binding specificity. The introduction of soluble anti-VEGFR2 to the imaging solution lead to a significant decrease in the number of recognitions sites over 60 min postblocking.

In addition, this nanoscale imaging showed that available VEGRFR2 receptors are nonuniformly distributed over 2-$\mu m^2$ regions, with a close spatial association to the underlying cortical cytoskeleton. This finding supports the current hypothesis that VEGRFR2 function is closely related to that of transmembrane integrin complexes transmitting force from the extracellular matrix to the actin cytoskeleton. Analysis of recognition images ($1.5 \times 1.5$ $\mu m^2$) indicated about 9.8 sites per $\mu m^2$ and hence about $1.5 \times 10^5$ VEGRFR2 receptors per cell. This determination of receptors among individual cells is in reasonable agreement with cell population–averaged measurements through radiolabelled ligands.

TREC images were also acquired with MAC tips coated with antibody anti-Kv11.1 (against epitope tags present on the human ether-á-go-go-related gene [hERG] subunits) via PEG linker (Figure 18.13A). The recognition map represents an amplitude reduction due to specific binding between anti-Kv11.1 on the tip and epitope tags on the cell surface (dark spots) (Figure 18.13B). These dark spots (amplitude reduction up to 2 nm) were distributed nonuniformly and reflect microdomains with dimensions from ~30 up to ~350 nm, with a mean $\pm$ SD of $99 \pm 81$ nm ($n = 25$) for the long domain axis. During several subsequent rescans recognition maps of hERG channels remained unchanged. Hereafter, ErgTx1 was very slowly (50 $\mu$L/min) injected in the fluid cell while scanning the same sample. After the first and second injection of ErgTx1 (concentration of ~400 nM), no visual change in the recognition maps was observed. However, the recognition clusters partly disappeared after the third injection of ErgTx1 (~1 $\mu$M), whereas no change in the topography image was observed. The specific binding between anti-Kv11.1 and cellular surface was abolished when free ErgTx1 molecules bound to the hERG channels and thus blocked the antibody access to interact with epitope tags on hERG subunits. The topography of a scanned cell surface areas shows a complex picture of linear and branched filamentous structures with some globular features. Most domains are found to be located near and between filaments. TREC results suggest that ErgTx1 not only interacts with the extracellular surface of the pore domain (S5–S6), but also might interact with the voltage-sensing domains (S1–S4) of the hERG $K^+$ channel. These findings indicate a possibly new binding site of ErgTx1 in the voltage-sensing domain of the hERG $K^+$ channel. TREC is a suitable method for obtaining information about the structure and function of hERG $K^+$ channels on the cellar surface. The outcome of this study reveals that voltage-sensing domains (S1–S4) of hERG $K^+$ channel might be one of the binding sites of ErgTx1.

## 18.5. Immunogold Imaging

Immunogold labels, well known in electron and optical microscopy, may also be useful for discriminating specific molecules on a biological sample. The idea is to first incubate the sample with monoclonal antibodies directed against specific constituents, then further incubate it with the corresponding gold-conjugated secondary antibodies, and finally image the

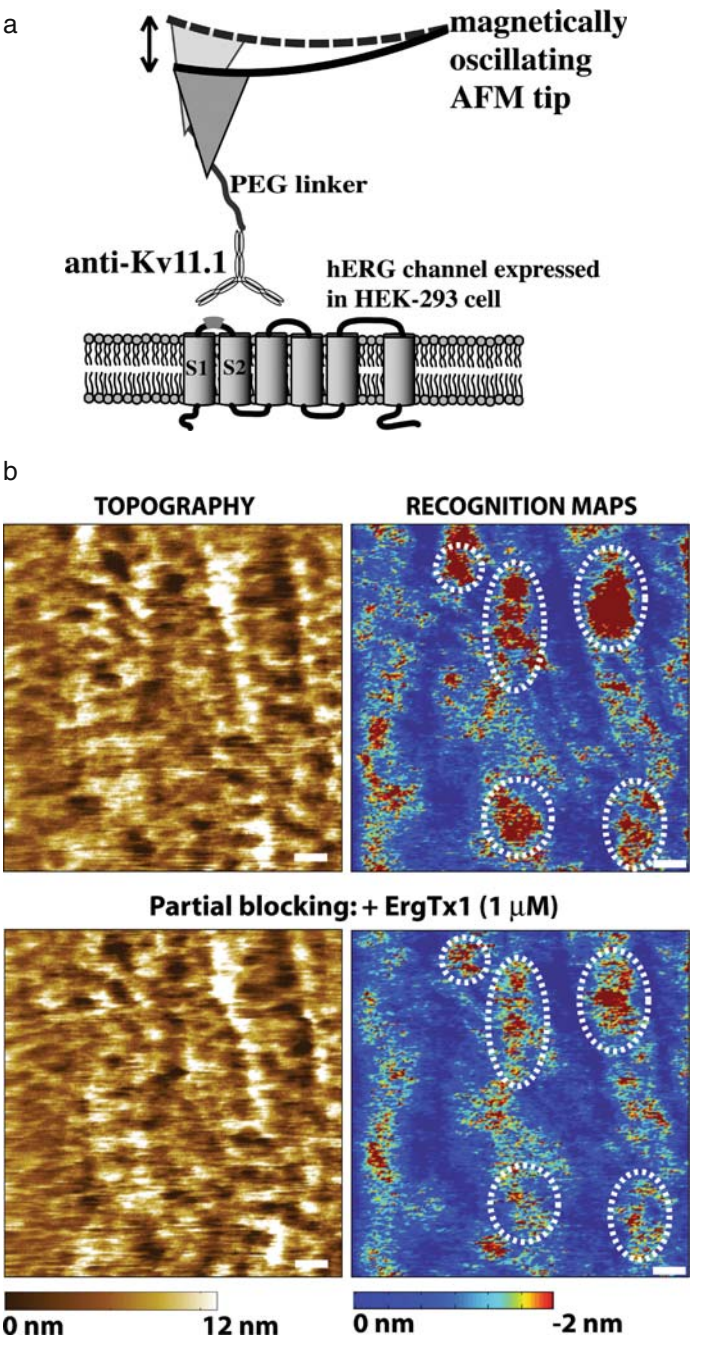


**Figure 18.13. A.** Schematic representation of recognition imaging to visualize human ether-á-go-go-related gene (hERG) $K^+$ channels (here binding sites at extracellular epitope between the S1 and S2 domains of hERG subunit [*light grey*]) on a gently fixed hERG HEK-293 cell surface. **B.** Topography and recognition imaging maps obtained on a hERG HEK-293 cell surface with anti-Kv11.1–functionalized tip. The most-pronounced recognition clusters are indicated by white lines. The presence of 400 nM ErgTx1 had practically no effect on the recognition map (data not shown), whereas the recognition clusters partly disappeared after the third injection of ErgTx1 (~1 μM). Blocking experiments do not affect membrane topography. Scale bars on all images are 170 nm. AFM, atomic force microscope; PEG, poly(ethylene glycol).

gold particles using AFM topographic imaging. The feasibility of using immunogold labels as cell-surface markers in AFM studies was first demonstrated on human lymphocytes [79]. Individual immunogold particles were clearly made visible on the cell surface, thus determining the location of antigens. More recently, a similar AFM-based immunogold technique revealed types I and II collagen fibers on rat fibroblasts and human chondrosarcoma cells [80]. Although well designed, these studies were performed in the dried state, which shows no clear benefit in using AFM over conventional immunogold electron microscopy.

Recently, this method was applied to hydrated bacteria, with the aim of localizing specific cell wall constituents (Figure 18.14) [15]. *M. bovis* BCG cells were treated with drugs to expose lipoarabinomannan (LAM) on the cell surface, then incubated with monoclonal anti-LAM antibodies, and further incubated with the corresponding gold-conjugated secondary antibodies. Images were obtained for native and treated cells, comparing contact and tapping (phase) modes. Gold particles were never seen in contact mode, emphasizing the need to use tapping (phase) mode for such *in situ* immunogold studies. With tapping mode, the surface

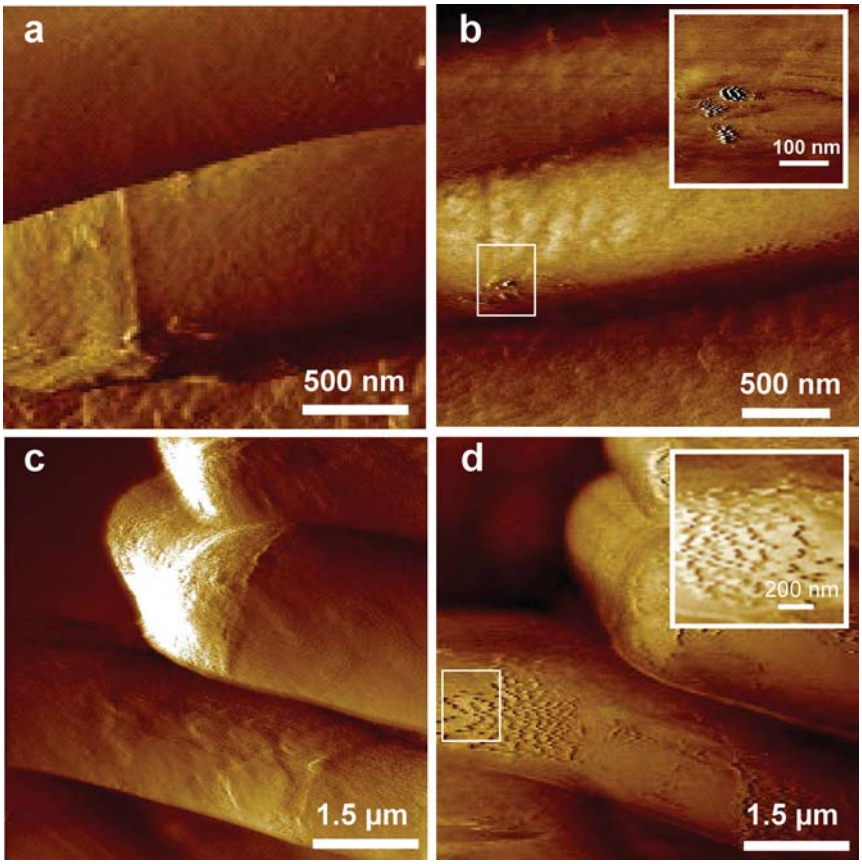


**Figure 18.14.** Localizing specific cell surface constituents by using immunogold atomic force microscopy. Contact mode (deflection) images **(A, C)** and tapping mode (phase) images **(B, D)** of immunogold-labelled *Mycobacterium bovis* bacillus Calmette-Guérin (BCG) cells. **A, B.** Native cells. **C, D.** Cells treated for 24 hr with isoniazid. All cells were incubated with monoclonal anti-lipoarabinomannan (LAM) antibodies, followed by another incubation with the corresponding gold-conjugated secondary antibodies. (Reprinted with permission from Alsteens et al. [15].)

of native cells showed essentially no labelling, indicating that LAM was not exposed at the surface. This finding was consistent with the uniform distribution of hydrophobic mycolic acids measured on native cells. By contrast, drug-treated cells revealed a substantial coverage of gold particles, indicating that LAM was exposed. Particles were poorly resolved and rather fuzzy in tapping mode, presumably reflecting energy dissipation of the oscillating tip. These observations, which correlate with topographic and CFM data, demonstrate that antimycobacterial drugs lead to the massive exposure of LAM at the cell surface, thereby contributing to our understanding of their action modes. Hence, tapping mode imaging of immunogold labels is a valuable approach for localizing specific antigens on biosurfaces.

## Acknowledgments

This work was supported by the National Foundation for Scientific Research (FNRS), the Université Catholique de Louvain (Fonds Spéciaux de Recherche), the Région Wallonne, the Federal Office for Scientific, Technical and Cultural Affairs (Interuniversity Poles of Attraction Programme), and the Research Department of the Communauté Française de Belgique (Concerted Research Action). YD and DA are Research Associate and Research Fellow of the FRS-FNRS, respectively. This work was further supported by the FFG program of the European Union projects Tips4Cells (LSHG-CT2005-512101), NASSAP (EC-STREP-13532), BioLightTouch (028181), and IMMUNANOMAP (MRTN-CT-2006-035946). AE and LC are Research Associates of the BioLigthTouch, and JT is Research Associate of the NASSAP project.

## References

1. Dufrêne, Y. F. 2008. Towards nanomicrobiology using atomic force microscopy. Nat. Rev. Microbiol. 6:674–680.
2. Engel, A., and D. J. Muller. 2000. Observing single biomolecules at work with the atomic force microscope. Nat. Struct. Biol. 7:715–718.
3. Gerber, C., and H. P. Lang. 2006. How the doors to the nanoworld were opened. Nat. Nanotechnol. 1:3–5.
4. Hinterdorfer, P., and Y. F. Dufrene. 2006. Detection and localization of single molecular recognition events using atomic force microscopy. Nat. Methods 3:347–355.
5. Müller, D. J., K. T. Sapra, S. Scheuring, A. Kedrov, P. L. Frederix, D. Fotiadis, and A. Engel. 2006. Single-molecule studies of membrane proteins. Curr. Opin. Struct. Biol. 16:489–495.
6. Burnham, N. A., X. Chen, C. S. Hodges, G. A. Matei, E. J. Thoreson, C. J. Roberts, M. C. Davies, and S. J. B. Tendler. 2003. Comparison of calibration methods for atomic-force microscopy cantilevers. Nanotechnology 14:1–6.
7. Frisbie, C. D., L. F. Rozsnyai, A. Noy, M. S. Wrighton, and C. M. Lieber. 1994. Functional-group imaging by chemical force microscopy. Science 265:2071–2074.
8. Noy, A. 2006. Chemical force microscopy of chemical and biological interactions. Surf. Interface Anal. 38:1429–1441.
9. Dufrêne, Y. F. 2008. Atomic force microscopy and chemical force microscopy of microbial cells. Nat. Protocols 3:1132–1138.
10. Alsteens, D., E. Dague, P. G. Rouxhet, A. R. Baulard, and Y. F. Dufrêne. 2007. Direct measurement of hydrophobic forces on cell surfaces using AFM. Langmuir 23:11977–11979.
11. Vezenov, D. V., A. Noy, L. F. Rozsnyai, and C. M. Lieber. 1997. Force titrations and ionization state sensitive imaging of functional groups in aqueous solutions by chemical force microscopy. J. Am. Chem. Soc. 119: 2006–2015.
12. Ahimou, F., F. A. Denis, A. Touhami, and Y. F. Dufrene. 2002. Probing microbial cell surface charges by atomic force microscopy. Langmuir 18:9937–9941.

13. Dague, E., D. Alsteens, J. P. Latge, C. Verbelen, D. Raze, A. R. Baulard, and Y. F. Dufrêne. 2007. Chemical force microscopy of single live cells. Nano Lett. 7:3026–3030.
14. Dague, E., D. Alsteens, J. P. Latgé, and Y. F. Dufrêne. 2008. High-resolution cell surface dynamics of germinating *Aspergillus fumigatus* conidia. Biophys. J. 94:656–660.
15. Alsteens, D., C. Verbelen, E. Dague, D. Raze, A. R. Baulard, and Y. F. Dufrêne. 2008. Organization of the mycobacterial cell wall: A nanoscale view. Eur. J. Physiol. 456:117–125.
16. Florin, E. L., V. T. Moy, and H. E. Gaub. 1994. Adhesion forces between individual ligand receptor pairs. Science 264:415–417.
17. Lee, G. U., D. A. Kidwell, and R. J. Colton. 1994. Sensing discrete streptavidin biotin interactions with atomic force microscopy. Langmuir 10:354–357.
18. Fritz, J., A. G. Katopodis, F. Kolbinger, and D. Anselmetti. 1998. Force-mediated kinetics of single P-selectin ligand complexes observed by atomic force microscopy. Proc. Natl. Acad. Sci. USA. 95:12283–12288.
19. Lee, G. U., L. A. Chrisey, and R. J. Colton. 1994. Direct measurement of the forces between complementary strands of DNA. Science 266:771–773.
20. Touhami, A., B. Hoffmann, A. Vasella, F. A. Denis, and Y. F. Dufrene. 2003. Probing specific lectin–carbohydrate interactions using atomic force microscopy imaging and force measurements. Langmuir 19:1745–1751.
21. Dammer, U., O. Popescu, P. Wagner, D. Anselmetti, H. J. Guntherodt, and G. N. Misevic. 1995. Binding strength between cell-adhesion proteoglycans measured by atomic force microscopy. Science 267:1173–1175.
22. Berquand, A., N. Xia, D. G. Castner, B. H. Clare, N. L. Abbott, V. Dupres, Y. Adriaensen, and Y. F. Dufrêne. 2005. Antigen binding forces of single antilysozyme Fv fragments explored by atomic force microscopy. Langmuir 21:5517–5523.
23. Dupres, V., F. D. Menozzi, C. Locht, B. H. Clare, N. L. Abbott, S. Cuenot, C. Bompard, D. Raze, and Y. F. Dufrêne. 2005. Nanoscale mapping and functional analysis of individual adhesins on living bacteria. Nat. Methods 2:515–520.
24. Hinterdorfer, P., W. Baumgartner, H. J. Gruber, K. Schilcher, and H. Schindler. 1996. Detection and localization of individual antibody–antigen recognition events by atomic force microscopy. Proc. Natl. Acad. Sci. USA 93:3477–3481.
25. Allen, S., X. Y. Chen, J. Davies, M. C. Davies, A. C. Dawkes, J. C. Edwards, C. J. Roberts, J. Sefton, S. J. B. Tendler, and P. M. Williams. 1997. Detection of antigen–antibody binding events with the atomic force microscope. Biochemistry 36:7457–7463.
26. Ong, Y. L., A. Razatos, G. Georgiou, and M. M. Sharma. 1999. Adhesion forces between *E-coli* bacteria and biomaterial surfaces. Langmuir 15:2719–2725.
27. Bowen, W. R., N. Hilal, R. W. Lovitt, and C. J. Wright. 1998. Direct measurement of the force of adhesion of a single biological cell using an atomic force microscope. Colloids Surf. A Physicochem. Eng. Asp. 136:231–234.
28. Lower, S. K., M. F. Hochella, and T. J. Beveridge. 2001. Bacterial recognition of mineral surfaces: Nanoscale interactions between *Schewanella* and alpha-FeOOH. Science 292:1360–1363.
29. Benoit, M., D. Gabriel, G. Gerisch, and H. E. Gaub. 2000. Discrete interactions in cell adhesion measured by single-molecule force spectroscopy. Nat. Cell Biol. 2:313–317.
30. Zhang, X. H., E. Wojcikiewicz, and V. T. Moy. 2002. Force spectroscopy of the leukocyte function-associated antigen-1/intercellular adhesion molecule-1 interaction. Biophys. J. 83:2270–2279.
31. Ebner, A., P. Hinterdorfer, and H. J. Gruber. 2007. Comparison of different aminofunctionalization strategies for attachment of single antibodies to AFM cantilevers. Ultramicroscopy 107:922–927.
32. Ros, R., F. Schwesinger, D. Anselmetti, M. Kubon, R. Schafer, A. Pluckthun, and L. Tiefenauer. 1998. Antigen binding forces of individually addressed single-chain Fv antibody molecules. Proc. Natl. Acad. Sci. USA 95:7402–7405.
33. Strunz, T., K. Oroszlan, R. Schafer, and H. J. Guntherodt. 1999. Dynamic force spectroscopy of single DNA molecules. Proc. Natl. Acad. Sci. USA 96:11277–11282.
34. Schumakovitch, I., W. Grange, T. Strunz, P. Bertoncini, H. J. Guntherodt, and M. Hegner. 2002. Temperature dependence of unbinding forces between complementary DNA strands. Biophys. J. 82:517–521.
35. Baumgartner, W., P. Hinterdorfer, W. Ness, A. Raab, D. Vestweber, H. Schindler, and D. Drenckhahn. 2000. Cadherin interaction probed by atomic force microscopy. Proc. Natl. Acad. Sci. USA 97:4005–4010.
36. Baumgartner, W., H. J. Gruber, P. Hinterdorfer, and D. Drenckhahn. 2000. Affinity of *trans*-interacting VE-cadherin determined by atomic force microscopy. Single Mol. 1:119–122.
37. Ludwig, M., W. Dettmann, and H. E. Gaub. 1997. Atomic force microscope imaging contrast based on molecular recognition. Biophys. J. 72:445–448.

38. Grandbois, M., W. Dettmann, M. Benoit, and H. E. Gaub. 2000. Affinity imaging of red blood cells using an atomic force microscope. J. Histochem. Cytochem. 48:719–724.
39. Lehenkari, P. P., G. T. Charras, A. Nykänen, and M. A. Horton. 2000. Adapting atomic force microscopy for cell biology. Ultramicroscopy 82:289–295.
40. Almqvist, N., R. Bhatia, G. Primbs, N. Desai, S. Banerjee, and R. Lal. 2004. Elasticity and adhesion force mapping reveals real-time clustering of growth factor receptors and associated changes in local cellular rheological properties. Biophys. J. 86:1753–1762.
41. Gilbert, Y., M. Deghorain, L. Wang, B. Xu, P. D. Pollheimer, H. J. Gruber, J. Errington, B. Hallet, X. Haulot, C. Verbelen, P. Hols, and Y. F. Dufrene. 2007. Single-molecule force spectroscopy and imaging of the vancomycin/D-Ala-D-Ala interaction. Nano Lett. 7:796–801.
42. Camesano, T. A., Y. Liu, and M. Datta. 2007. Measuring bacterial adhesion at environmental interfaces with single-cell and single-molecule techniques. Adv. Water Resour. 30:1470–1491.
43. Alsteens, D., V. Dupres, K. Mc Evoy, L. Wildling, H. J. Gruber, and Y. F. Dufrêne. 2008. Structure, cell wall elasticity and polysaccharide properties of living yeast cells, as probed by AFM. Nanotechnology, 19:384005(9pp).
44. Francius, G., S. Lebeer, D. Alsteens, L. Wildling, H. J. Gruber, P. Hols, S. De Keersmaecker, J. Vanderleyden, and Y. F. Dufrêne. 2008. Detection, localization and conformational analysis of single polysaccharide molecules on live bacteria. ACS Nano, 2:1921–1929.
45. Sotres, J., A. Lostao, L. Wildling, A. Ebner, C. Gomez-Moreno, H. J. Gruber, P. Hinterdorfer, and A. M. Baro. 2008. Unbinding molecular recognition force maps of localized single receptor molecules by atomic force microscopy. Chemphyschem 9:590–599.
46. Ebner, A., F. Kienberger, G. Kada, C. M. Stroh, M. Geretschlager, A. S. M. Kamruzzahan, L. Wildling, W. T. Johnson, B. Ashcroft, J. Nelson, S. M. Lindsay, H. J. Gruber, and P. Hinterdorfer. 2005. Localization of single avidin–biotin interactions using simultaneous topography and molecular recognition imaging. Chemphyschem 6:897–900.
47. Kienberger, F., A. Ebner, H. J. Gruber, and P. Hinterdorfer. 2006. Molecular recognition imaging and force spectroscopy of single biomolecules. Acc. Chem. Res. 39:29–36.
48. Stroh, C., H. Wang, R. Bash, B. Ashcroft, J. Nelson, H. Gruber, D. Lohr, S. M. Lindsay, and P. Hinterdorfer. 2004. Single-molecule recognition imaging microscopy. Proc. Natl. Acad. Sci. USA 101:12503–12507.
49. Chtcheglova, L. A., F. Atalar, U. Ozbek, L. Wildling, A. Ebner, and P. Hinterdorfer. 2008. Localization of the ergtoxin-1 receptors on the voltage sensing domain of hERG K+ channel by AFM recognition imaging. Pflugers Arch. Eur. J. Physiol. 456:247–254.
50. Chtcheglova, L. A., J. Waschke, L. Wildling, D. Drenckhahn, and P. Hinterdorfer. 2007. Nano-scale dynamic recognition imaging on vascular endothelial cells. Biophys. J. 93:L11–13.
51. Ebner, A., D. Nikova, T. Lange, J. Haeberle, S. Falk, A. Duebbers, R. Bruns, P. Hinterdorfer, H. Oberleithner, and H. Schillers 2008. Determination of CFTR densities in erythrocyte plasma membranes using recognition imaging. Nanotechnology19:384017.
52. Stroh, C. M., A. Ebner, M. Geretschlager, G. Freudenthaler, F. Kienberger, A. S. M. Kamruzzahan, S. J. Smith-Gill, H. J. Gruber, and P. Hinterdorfer. 2004. Simultaneous topography and recognition imaging using force microscopy. Biophys. J. 87:1981–1990.
53. Ebner, A., L. Wildling, R. Zhu, C. Rankl, T. Haselgrubler, P. Hinterdorfer, and H. J. Gruber. 2007. Funtionalization of probe tips and supports for single-molecule recognition force microscopy. Top Curr. Chem 285:29–76.
54. Liu, Y. Z., S. H. Leuba, and S. M. Lindsay. 1999. Relationship between stiffness and force in single molecule pulling experiments. Langmuir 15:8547–8548.
55. Lin, L., H. Wang, Y. Liu, H. Yan, and S. Lindsay. 2006. Recognition imaging with a DNA aptamer. Biophys. J. 90:4236–4238.
56. Lin, L., D. Hom, S. M. Lindsay, and J. C. Chaput. 2007. *In vitro* selection of histone h4 aptamers for recognition imaging microscopy. J. Am. Chem. Soc. 129:14568–14569.
57. Sleytr, U. B., C. Huber, N. Ilk, D. Pum, B. Schuster, and E. M. Egelseer. 2007. S-layers as a tool kit for nanobiotechnological applications. FEMS Microbiol. Lett. 267:131–144.
58. Sleytr, U. B., M. Sara, D. Pum, and B. Schuster. 2001. Characterization and use of crystalline bacterial cell surface layers. Prog. Surf. Sci. 68:231–278.
59. Sleytr, U. B., and T. J. Beveridge. 1999. Bacterial S-layers. Trends Microbiol. 7:253–260.
60. Sleytr, U. B., P. Messner, D. Pum, and M. Sara. 1999. Crystalline bacterial cell surface layers (S layers): From supramolecular cell structure to biomimetics and nanotechnology. Angew. Chem. Int. Ed. 38:1035–1054.
61. Sleytr, U. B., E. M. Egelseer, N. Ilk, D. Pum, and B. Schuster. 2007. S-Layers as a basic building block in a molecular construction kit. FEBS J. 274:323–334.

62. Voss, S., and A. Skerra. 1997. Mutagenesis of a flexible loop in streptavidin leads to higher affinity for the Strep-tag II peptide and improved performance in recombinant protein purification. Protein Eng. 10:975–982.
63. Ilk, N., P. Kosma, M. Puchberger, E. M. Egelseer, H. F. Mayer, U. B. Sleytr, and M. Sára. 1999. Structural and functional analyses of the secondary cell wall polymer of *Bacillus sphaericus* CCM 2177 that serves as an S-layer specific anchor. J. Bacteriol. 181:7643–7646.
64. Pleschberger, M., A. Neubauer, E. M. Egelseer, S. Weigert, B. Lindner, U. B. Sleytr, S. Muyldermans, and M. Sara. 2003. Generation of a functional monomolecular protein lattice consisting of an S-layer fusion protein comprising the variable domain of a camel heavy chain antibody Bioconjug. Chem. 14:440–448.
65. Tang, J., A. Ebner, N. Ilk, H. Lichtblau, C. Huber, R. Zhu, D. Pum, M. Leitner, V. Pastushenko, H. J. Gruber, U. B. Sleytr, and P. Hinterdorfer. 2007. High-affinity tags fused to S-layer proteins probed by atomic force microscopy. Langmuir 24:1324–1329.
66. Ebner, A., F. Kienberger, G. Kada, C. M. Stroh, M. Geretschlager, A. S. Kamruzzahan, L. Wildling, W. T. Johnson, B. Ashcroft, J. Nelson, S. M. Lindsay, H. J. Gruber, and P. Hinterdorfer. 2005. Localization of single avidin–biotin interactions using simultaneous topography and molecular recognition imaging. Chemphyschem 6:897–900.
67. Schwiebert, E. M., D. J. Benos, and C. M. Fuller. 1998. Cystic fibrosis: A multiple exocrinopathy caused by dysfunctions in a multifunctional transport protein. Am. J. Med. 104:576–590.
68. Braunstein, G. M., R. M. Roman, J. P. Clancy, B. A. Kudlow, A. L. Taylor, V. G. Shylonsky, B. Jovov, K. Peter, T. Jilling, Ismailov, II, D. J. Benos, L. M. Schwiebert, J. G. Fitz, and E. M. Schwiebert. 2001. Cystic fibrosis transmembrane conductance regulator facilitates ATP release by stimulating a separate ATP release channel for autocrine control of cell volume regulation. J. Biol. Chem. 276:6621–6630.
69. Dupuit, F., N. Kalin, S. Brezillon, J. Hinnrasky, B. Tummler, and E. Puchelle. 1995. CFTR and differentiation markers expression in non-CF and delta-F-508 homozygous CF nasal epithelium. J. Clin. Invest. 96:1601–1611.
70. Kalin, N., A. Claass, M. Sommer, E. Puchelle, and B. Tummler. 1999. Delta F508 CFTR protein expression in tissues from patients with cystic fibrosis. J. Clin. Invest. 103:1379–1389.
71. Lange, T., P. Jungmann, J. Haberle, S. Falk, A. Duebbers, R. Bruns, A. Ebner, P. Hinterdorfer, H. Oberleithner, and H. Schillers. 2006. Reduced number of CFTR molecules in erythrocyte plasma membrane of cystic fibrosis patients. Mol. Membr. Biol. 23:317–323.
72. Sprague, R. S., M. L. Ellsworth, A. H. Stephenson, M. E. Kleinhenz, and A. J. Lonigro. 1998. Deformation-induced ATP release from red blood cells requires CFTR activity. Am. J. Physiol. Heart Circ. Physiol. 275:H1726–H1732.
73. Sterling, K. M., S. Shah, R. J. Kim, N. I. F. Johnston, A. Y. Salikhova, and E. H. Abraham. 2004. Cystic fibrosis transmembrane conductance regulator in human and mouse red blood cell membranes and its interaction with ecto-apyrase. J. Cell. Biochem. 91:1174–1182.
74. Stumpf, A., J. Almaca, K. Kunzelmann, K. Wenners-Epping, S. M. Huber, J. Haberle, S. Falk, A. Duebbers, M. Walte, H. Oberleithner, and H. Schillers. 2006. IADS, a decomposition product of DIDS activates a cation conductance in *Xenopus* oocytes and human erythrocytes: New compound for the diagnosis of cystic fibrosis. Cell. Physiol. Biochem. 18:243–252.
75. Stumpf, A., K. Wenners-Epping, M. Walte, T. Lange, H. G. Koch, J. Haberle, A. Dubbers, S. Falk, L. Kiesel, D. Nikova, R. Bruns, H. Bertram, H. Oberleithner, and H. Schillers. 2006. Physiological concept for a blood based CFTR test. Cell. Physiol. Biochem. 17:29–36.
76. Verloo, P., C. H. M. Kocken, A. Van der Wel, B. C. Tilly, B. M. Hogema, M. Sinaasappel, A. W. Thomas, and H. R. De Jonge. 2004. *Plasmodium falciparum*-activated chloride channels are defective in erythrocytes from cystic fibrosis patients. J. Biol. Chem. 279:10316–10322.
77. Vincent, P. A., K. Xiao, K. M. Buckley, and A. P. Kowalczyk. 2004. VE-cadherin: Adhesion at arm's length. AJP Cell Physiol. 286:C987–997.
78. Lee, S., J. Mandic, and K. J. Van Vliet. 2007. Chemomechanical mapping of ligand–receptor binding kinetics on cells. Proc. Natl. Acad. Sci. USA 104:9609–9614.
79. Putman, C. A. J., B. G. Degrooth, P. K. Hansma, N. F. Vanhulst, and J. Greve. 1993. Immunogold labels: Cell-surface markers in atomic force microscopy. Ultramicroscopy 48:177–182.
80. Arntz, Y., L. Jourdainne, G. Greiner-Wacker, S. Rinckenbach, J. Ogier, J. C. Voegel, P. Lavalle, and D. Vautier. 2006. Immunogold detection of types I and II chondrocyte collagen fibrils: An *in situ* atomic force microscopic investigation. Microsc. Res. Tech. 69:283–290.